REFRACTIVE INDEX TUNING WITH BURSTEIN-MOSS EFFECT IN INDIUM NITRITE UNDER PHOTOEXCITATION

A THESIS

SUBMITTED TO THE PROGRAM OF PHYSICS

AND THE INSTITUTE OF ENGINEERING AND SCIENCE

OF BILKENT UNIVERSITY

IN PARTIAL FULFILLMENT OF THE REQUIREMENTS

FOR THE DEGREE OF

MASTER OF SCIENCE

By

Cem Murat Turgut

August, 2009

I certify that I have read this thesis and that in my opinion it is fully adequate, in scope and in quality, as a thesis for the degree of Master of Science.

Assoc. Prof. Dr. Ceyhun Bulutay (Advisor)

I certify that I have read this thesis and that in my opinion it is fully adequate, in scope and in quality, as a thesis for the degree of Master of Science.

Prof. Dr. Atilla Aydınlı

I certify that I have read this thesis and that in my opinion it is fully adequate, in scope and in quality, as a thesis for the degree of Master of Science.

Prof. Dr. Raşit Turan

Approved for the Institute of Engineering and Science:

Prof. Dr. Mehmet B. Baray
Director of the Institute Engineering and Science

ABSTRACT

REFRACTIVE INDEX TUNING WITH BURSTEIN-MOSS EFFECT IN INDIUM NITRITE UNDER PHOTOEXCITATION

Cem Murat Turgut
M.S. in Physics
Supervisor: Assoc. Prof. Dr. Ceyhun Bulutay
August, 2009

The band filling effect due to free carriers introduces a shift in the absorption edge, which in turn modifies the refractive index of the medium through the Kramers-Kronig relation. This is known as the Burstein-Moss effect. Based on the full band pseudopotential electronic structure calculations, we demonstrate that Burstein-Moss effect will be crucial in the design of InN based lasers. The primary reason is the small effective mass and the strong nonparabolicity of the conduction band of InN where the shift in the absorption edge is more than 0.5 eV for an electron density of the order of 10^{19} cm^{-3}. On the other hand, for the case of valence band, the shift in the absorption edge is approximately 0.04 eV. However due to high density of states at the edge of the valence band, also this shift becomes crucial since it opens intraband transitions in the medium. In the case of laser structures, the Burstein-Moss effect in both conduction and valence bands needs to be considered. Furthermore, we take into account the band gap renormalization due to high free carrier concentration. For the case of semiconductor laser structures, which can be also considered as an n-p junction, we predict about 2% change in the refractive index for a wavelength 1.55 μm at an electron-hole density of 10^{19} cm^{-3}. When we compare photoexcited (i.e., $n = p$) InN with n-type doped InN, in the former case the intraband transitions in the valence band which is a result of $\Gamma_5^v \rightarrow \Gamma_6^v$ transition, partially cancels the Burstein-Moss effect. Our findings can also have direct implications for InN based optical modulators.

Keywords: Refractive index change, semiconductor optics, band filling, band gap renormalization.

ÖZET

IŞIK UYARIMI ALTINDA İNDİYUM NİTRAT' IN BURSTEIN-MOSS ETKİSİYLE KIRINIM İNDİSİNDEKİ DEĞİŞİM

Cem Murat Turgut
Fizik, Yüksek Lisans
Tez Yöneticisi: Doç. Dr. Ceyhun Bulutay
Ağustos, 2009

Serbest taşıyıcılar sebebiyle oluşan band dolum etkisi, soğurma eşiğinde kaymaya sebep olur ve bu değişiklik, Kramers-Kronig ilişkisiyle, maddenin kırınım indisini değiştirir. Bu, Burstein Moss etkisi olarak da bilinir. Tüm Brillouin bölgesi boyunca elektronik bant yapısı görünür potansiyel yaklaşımıyla elde edilmiştir ve bu hesaplamalara dayanarak, InN temelli lazerlerin tasarımında Burstein Moss etkisinin can alıcı olduğu gösterilmiştir. İletkenlik bant kenarındaki parabolik olmayan enerji dağınım bağıntısı ve küçük etkin kütle, bu etkinin en başta gelen sebeplerindendir. 10^{19} cm^{-3} mertebesindeki elektron yoğunluğu iletkenlik bandının soğurma eşiğinde, 0.5 eV'tan daha fazla kaymaya sebep olur. Değerlik bandında bu değer 0.04 eV olmasına rağmen, bant kenarındaki yüksek durum yoğunluğu, soğurma eşiğindeki bu küçük kaymayı önemli kılmaktadır. Lazer yapılarında, Burstein Moss etkisi hem iletkenlik hem de değerlik bandı göz önüne alarak değerlendirilmelidir. Buna ilaveten, yüksek yoğunluktaki serbest taşıyıcılar bant aralığında daralmaya neden olur. Bütün bu etkilerin yanında plazma etkisi de hesaba katılarak, kırınım indisindeki değişim hesaplanmıştır. Burstein Moss etkisiyle, tipik lazer dalgaboyu olan 1.55 μm'de, yarıiletken maddenin kırınım indisinde yaklaşık 2% değişim tahmin ediyoruz. Sonuçlarımızı n-tipi InN ile karşılaştırdığımızda, $\Gamma_5^v \rightarrow \Gamma_6^v$ geçişinden kaynaklanan yoğun bant içi geçişleri n-p tipi InN'ta Burstein Moss etkisini kısmen kaybettirmektedir. Bulgularımızın, InN temelli optik modülatörler için de ilgili olacağı düşünülmektedir.

Anahtar sözcükler: Kırınım indis değişimi, yarıiletken optiği, bant dolumu, bant aralığında daralma.

Acknowledgement

I am very glad to thank Assoc. Prof. Dr. Ceyhun Bulutay who has been a great support in the process of my thesis. He is beyond a thesis supervisor. I take him as a role model in my career. Moreover, I am grateful to my group members for the fish sandwiches. I would like to thank Halime Kutlutan for the language support, Levent Subaşı for Linux support, Ümit Keleş and Duygu Can for friendly conversations, Emre Taşgın for tea services, Kurtuluş Abak for being a co-pilot in our trips, Hasan Şahin for the cold beverages. I send lots of love to Ceydos, Deniz and Engin who have been great online supports. I would like to thank my family for being great supporters of my continuing to be an academician, and I would like to mention that there are many names that I do not forget but cannot write here. It would be a very long list then.

The financial support by the UNAM-Regpot Project (Grant No:203953) for attending the E-MRS conference in June 2009 is acknowledged.

This thesis is dedicated to Tuğçe, who has stood up to the difficulties throughout my undergraduate and master life with me.

Contents

List of Figures

List of Tables

Chapter 1

Introduction

1.1 Band Filling Effect

The history behind this thesis goes back to 1950's. The first problem is encountered with the Indium including compounds in 1953. The measured band gap (ΔE_g) of Indium Antimonide (InSb) had divergent values. Tatenbaum and Briggs tried to explain this anomalous behaviour of InSb [1]. For different concentration of impurity levels, they measured different band gap values by means of photo absorption experiment and according to their measurement they concluded that the reason for this anomalous behaviour was related to the impurities however, they couldn't explain the physical reasons [1].

In the same year 1953, Burstein remeasured the band gap of InSb [2], and he also confirmed the absorption values for InSb reported by Tatenbaum and Briggs' work. However, he explained the anomalous band gap behaviour with a different perspective. The reason was explained as being due to the small effective mass of InSb rather than an impurity effect. The sharp curvature in the bottom of the conduction band results in the small electron effective mass and small density of states at that region. For the relatively small electron densities, the Fermi level of the semiconductor lies above the conduction band as a result of filling available density of states and the Fermi level increases rapidly with the

increasing electron density [2]. As the carrier density increases, the absorption energy from valence band to Fermi energy level increases. At the same time, Moss independently proposed the same reason for the unusual band gap of InSb [3]. Hence this is named as the Burstein Moss effect which is generally observed in the semiconductors which have small effective masses. The importance of this effect for applied physics is realized in 1960's, as it gives a chance to obtain different optical properties with the same semiconductor.

1.2 Burstein-Moss Effect in Semiconductor Physics

By doping the semiconductor, one can modulate the absorption edge, refractive index, emission of the medium by means of Burstein-Moss effect. In 1969, Dapkus and his colleagues modulated the laser transition energies and wavelength limits of GaAs by n-type doping [4]. With a doping level $N_d \sim 10^{18}$ donors/cm^3, photon energy of emitted laser light increases rapidly. This is because the Fermi level in the conduction band moves up with the doping level. Interband recombination processes predominantly occur from the Fermi level in the conduction band to the valence band edge. So n-type semiconductor lasers lase at higher energies compared to the undoped semiconductor lasers. On the other hand, the effect of donors and the acceptors in the band structure should be considered since they can open new transition levels in the forbidden gap of the medium [4].

The effect of band filling on the absorption coefficient is calculated for GaAs based lasers in Bell Laboratories in 1975 [5]. The measurements were made on highly doped n-type samples with a free electron concentration $\sim 6.7\times10^{18}$ cm^{-3}. By using the reflectance data, together with the Kramers-Kronig relation, they obtained the absorption coefficient. The result showed that absorption is strongly dependent on the impurity concentration. A similar work was done in 2001 for InSb [6]. Through the Kramers-Kronig relations carrier dependent absorption spectra and the refractive index change is calculated in correction to the laser structures. Compared to the intrinsic semiconductor, high doping tends to reduce

the refractive index [6].

In 1989, Schubert applied Burstein Moss effect to the quarter wave semiconductor plates of InP-InGaAs. As the carrier density increased, they filled the available states in the conduction band for n-type semiconductors. As a result of band filling, states at the bottom of the conduction band were blocked, so the electron excitation from valence band to these states was reduced for a photon energy with corresponding wavelength. So the reflectivity at this wavelength was increased [7]. This effect was used for passive mode locking and Q switching of an erbium laser at a wavelength 3 μm by using InAs. At room temperature band gap of InAs is 0.35 eV which corresponds a wavelength 3.54 μm however n-type InAs shows a band to band transitions at 0.44 eV with a wavelength 2.8 μm [8]. Also in the same year, this effect was used to modulate the waveguide in a two dimensional system. Junction field-effect transistor was incorporated to an optical waveguide and the gates modulated the light by band filling effect. By applying reverse gate-source bias V_{gs} and drain-source bias V_{ds}, free carriers doped the waveguide, and as the free carrier concentration increased band filling effect was observed. As a result the absorption and the refractive index of the medium was modulated [9].

A more recent application of band filling effect was published in 2007 by Yang. Mercury-cadmium-telluride (HgCdTe) is an important semiconductor which is used for infrared photodetectors. By doping the material n-type, the luminescence peak of the semiconductor showed a blue shift with an amount of $\sim$ 40 meV [10]. These are the examples of Burstein-Moss effect which are used in semiconductor physics.

1.3 Band Filling Effect in InN

Band filling effect can be observed in the semiconductors which have small electron effective masses and low density of states at the conduction band edge. As it is seen above, In-included compounds are the best candidates for this effect.

Indium is a III-A group member in periodic table and makes compounds with V-A group members. In the last decades III-V semiconductors have been the focus of the attention of the semiconductor physics society because it has a wide range technological applications. Especially III-nitrite semiconductors attract attention for gallium nitride's applications in optoelectronics. Among III-nitrite semiconductors, InN has been of of interest in recent years.

InN preserved its mysteries for decades. Like InSb, the band gap of InN exhibits an anomalous behaviour. This effect first was observed in InN by Trainor and Rose [11] in 1974 and between 1985-86 it was intensively studied by Tansley and Foley for InN films growth by RF sputtering [12]. The increase in the absorption edge was empirically fitted as

$$E_g^m = E_g + 2.1 \times 10^{-8} n^{1/3} \text{ eV},$$

where E_g^m is the measured apparent band gap and n is the carrier concentration in cm^{-3}. They stated that band gap of the InN, $E_g = 1.9$ eV. This value had been commonly accepted for 15 years. In 2002, Wu and his colleagues characterised wurtzite InN grown by molecular beam epitaxy. By using optical absorption, photoluminescence and photomodulated reflectance techniques, they reported the unusual value of band gap of InN as 0.7 and 0.8 eV [13]. So the accepted value 1.9 eV is revised to 0.7 eV after 15 years!

This major band gap revision stems from the challenges in the growth of InN; the unintentionally doped (as grown) samples turn out to be highly n-doped [14]. So because of this unintentional n-type doping Burstein Moss effect occurs naturally. This revised band gap of InN is of interest since it has compatible value with the telecommunication wavelength at 1.55 μm which corresponds to 0.8 eV.

1.4 Modulator Applications

The main aim of the electro-optic devices is to alter the optical properties of the medium with an applied voltage. This applied voltage leads us a controllable

system over the device and in particular it changes the permittivity tensor and so the refractive index. With this change, the parameters of the waveguide such as phase, amplitude, frequency can be modulated. Therefore, understanding the response of the medium due to the applied field is crucial to the design electro-optic devices.

An electro-optic modulator is a device which is widely used in semiconductor physics. Basically, for the construction of the modulator, an electro-optic medium is sandwiched between a pair of electrodes which can be also modelled as a capacitor. The working principle is based on the electrically induced change in the refractive index or birefringence. These devices are generally designed for a single wavelength for the optimum performance. We can classify an electro-optic modulator into two types depending on the direction of applied voltage relative to the propagation direction of the light: transverse modulator for the proportional direction of the applied voltage and longitudinal modulator for the parallel configuration [15]. Phase modulators, polarization modulators and the amplitude modulators are the main types of the electro-optic modulators.

1.5 Plan of the Thesis

In the following chapters we will give a brief review of electro-optic and electro-absorption effects followed by essential technical preliminaries to compute the optical response of InN. Finally, including relevant effects such as band gap renormalization and free-carrier (plasma) refractive index contributions, we will try to explore the response of InN for a high photoexcitation introducing electon-hole pairs with densities $\sim 10^{18} - 10^{20}$ cm^{-3} which has great potential for the implementation of semiconductor lasers as well as optical modulators.

Chapter 2

Electro-Optic and Electro-Absorption Effects

When we apply a low frequency or steady electric field to a material, the optical properties of the material changes in response to this field. The applied electric field reorients the electronic orbitals, ions, and permanent dipoles in the material which induces an electric polarization. This induced polarization modifies the *refractive index* of the material. Such changes in the refractive index of the material in response to an electric field is called the *electro-optic effect*. On the other hand, the applied field can also change the absorption edge of the both bulk materials and quantum confined systems. These modifications in the band gap of the materials are known as *electro-absorption effects*. However, it should be mentioned that the changes in the refractive index and the absorption coefficient are intimately related to each other through the Kramers-Kronig relation. The physical reason behind it is the *causality principle*. More on this will be given in the following chapters. The purpose of this chapter is to give an overview of the electro-optic and electro-absorption effects.

2.1 Electro-Optic Effects

In materials without an inversion symmetry also called antisymmetric (such as bulk Group III-V compounds), the change in the refractive index is linearly proportional with the applied electric field. This effect is known linear electro-optic effect or *Pockels Effect*. However, if the material has an inversion symmetry (such as bulk Group IV compounds) the Pockels effect trivially vanishes and the electric field quadratically changes the refractive index which is known as *Kerr Effect*. Kerr Effect is masked by the much larger Pockels effect in antisymmetric materials. The refractive index change of the electro-optic medium is typically small. However if the wave propagates through this medium for a distance exceeding its wavelength, the phase of the wave can be modified significantly. One of the main motivation for changing the refractive index through the applied electric field is to design electrically controllable optical devices [16]. More details are provided below.

2.2 Pockels Effect

If we apply an electric field to the antisymmetric crystal in a general direction, the *dielectric impermeability* $(1/n^2)_i$ changes linearly depending on the the electric field. By using the 6×3 *electro-optic tensor* $\mathbf{r}$, we can evaluate the changes in the coefficients,

$$\Delta(\frac{1}{n^2})_i = \sum_{j=1}^{3} r_{ij} E_j \quad i = 1, \ldots, 6 \quad ; j = 1, 2, 3 = x, y, z,$$

where $\mathbf{r}_{ij}$ is the ij^{th} element of the linear electro-optic tensor [17].

Now we define a wave propagating in the x_3 direction and we apply an electric field along the x_1 direction. The *electro-optic tensor* for this configuration is described by the following equation,

$$(\frac{1}{n_1^2} + r_{11}E_1)x_1^2 + (\frac{1}{n_2^2} + r_{21}E_1)x_2^2 + 2r_{61}E_1 x_1 x_2 = 0.$$

Since the term containing r_{61} is responsible for the refractive index change in the x_1 direction, we can ignore this term for a moment.

$$\frac{1}{(n_1 + \Delta n_1)^2} = (\frac{1}{n_1^2} + r_{11}E_1),$$

For the electric fields lower than 20 kV/cm, $\mathcal{O}[\Delta n] \approx 10^{-4}$ so $\Delta n_1 \ll n_1$. For this approximation we can expand the formula as

$$\frac{1}{(n_1 + \Delta n_1)^2} \approx \frac{1}{n_1^2} - \frac{2\Delta n_1}{n_1^3} = (\frac{1}{n_1^2} + r_{11}E_1).$$

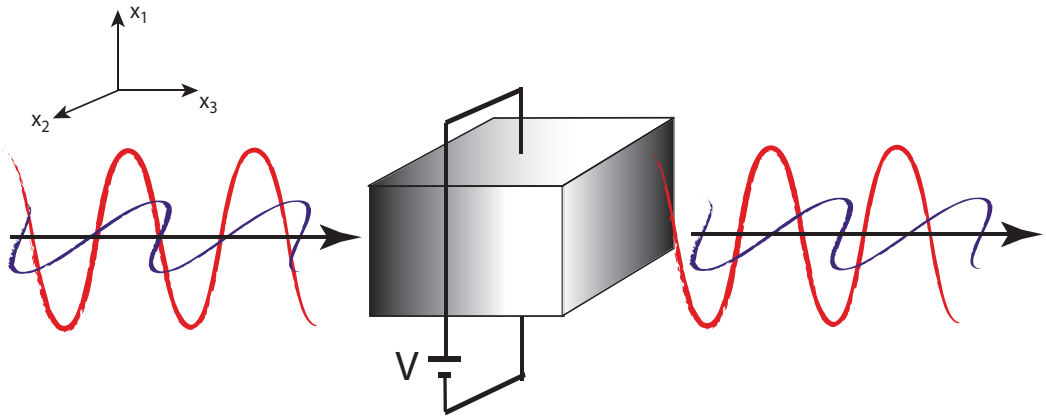

Figure 2.1: Basic illustration of an passing light though the electro-optic medium which is modulated by an external voltage.

The corresponding index change along the x_1 direction is,

$$\Delta n_1 \approx -\frac{n_1^3 r_{11} E_1}{2}.$$

Making the same assumption we can get the index change along x_2 direction as,

$$\Delta n_2 \approx -\frac{n_2^3 r_{21} E_1}{2}.$$

A polarized light wave propagating along the x_3 direction can be decomposed into two component: one along the x_2 direction and the other along the x_1 direction. We can define these waves as follows

$$E(x_2) = A_2 \exp\left[i\left(\omega t - k_0 n_2 x_3\right)\right], \quad E(x_1) = A_1 \exp\left[i(\omega t - k_0 n_1 x_3)\right],$$

k_0 is the wave number in free space. When the light covers a distance L in the electro-optic medium, a relative phase shift is observed between these orthogonal polarized components and this shift depends on $n_i\,(i = 1\,\text{or}\,2)$. After the propagation with a distance L in the x_3 direction in the crystal, the phase shift is,

$$\Delta\phi_1 = -k_0 L\left[n_2 - (n_2 + \Delta n_2)\right] = -\frac{k_0 n_2^3 r_{21} E_1 L}{2},$$

$$\Delta\phi_2 = -k_0 L\left[n_1 - (n_1 + \Delta n_1)\right] = -\frac{k_0 n_1^3 r_{11} E_1 L}{2}.$$

This calculation is done for the steady electric field. For the sinusoidally varying time dependent electric field E_1, the phase shift between these components also vary sinusoidally. As a result phase modulation will occur [15].

2.3 Kerr Effect

In 1876 John Kerr (1824-1907) stated that under the influence of the electric field, *isotropic* materials show *uniaxial* behaviour. The uniaxial materials show two different refractive indices for the propagation direction (extraordinary index n_e) and normal to the propagation direction (ordinary index n_o). As a result of this index difference for these directions, a birefringence is observed. This phenomena is named as the Kerr effect. This effect is distinguished from the preceding Pockels effect with a quadratic electric field dependence [15]. Impermeability tensor $(1/n^2)$ is defined as the the inverse dielectric constant. The changes in the refractive index according to the applied electric field is evaluated by using the 6×6 impermeability tensor ρ. To simplify the calculations, we use a coordinate system along the principal axes. So all the terms of the tensor become zero except the diagonal terms

$$\rho_{11} = \rho_{22} = \rho_{33} = \rho.$$

The applied electric field is in the z direction $E_1 = E_2 = 0, E_3 = E$. The refractive index parallel to the electric field in terms of ρ and the refractive index of the

isotropic medium n is defined as

$$\frac{1}{n^2}_{\parallel} = \frac{1}{n_e^2} = \frac{1}{n^2} + \rho E^2.$$

Since the electric field is applied in one direction, the refractive index of the ordinary axis does not change and remains the same

$$\frac{1}{n^2}_{\perp} = \frac{1}{n_o^2} = \frac{1}{n^2}.$$

As a result, the presence of the electric field changes the property of the isotropic medium and the medium shows uniaxial crystal behaviour with an optical axis parallel to the electric field. Again we assume that the change in the refractive index n_0 is small compared to n_e, so that we can use the binomial expansion to write

$$\frac{1}{n_e^2} = \frac{1}{(n_0 + \Delta n_0)^2} = \frac{1}{n_0^2} - \frac{2\Delta n_0}{n_0^3} = \frac{1}{n_0^2} + \rho E^2.$$

Refractive index difference between the ordinary and extraordinary axes can be measured by means of the induced birefringence and it is experimentally expressed as

$$\Delta n = K E^2 \lambda,$$

where K is called the Kerr constant. When the polarized light passes through the Kerr medium a phase difference between the ordinary and extraordinary axes occurs which is formulated as

$$\Gamma = 2\pi \frac{\Delta n L}{\lambda} = 2\pi K E^2 L.$$

By putting k_0 and Δn instead of $\frac{2\pi}{\lambda}$ and $(n_e - n_o)$, we can reformulate the above expression.

$$\begin{aligned} \Gamma &= k_0(n_e - n_0)L \\ &= k_0(n_0 + \Delta n_0 - n_0)L \\ &= \frac{2\pi}{\lambda}\Delta n_0 L \\ &= \frac{\pi}{\lambda} n_0^3 \rho E^2. \end{aligned}$$

By matching the theoretical and experimental expressions we can extract the Kerr constant as

$$K = \frac{n_0^3 \rho}{2\lambda}.$$

As a special case, to get a phase shift of $\Gamma = \pi$ for a medium with thickness d and length L half wave voltage is defined [15] as

$$V_{\frac{\lambda}{2}} = \frac{d}{\sqrt{2KL}}.$$

Electro-Absorption Effects

Absorption of the incident light near the band gap of the photonic material has a significant advantage to modulate the light. By externally applied electric field, the absorption characteristics of both bulk semiconductors and multi quantum well structures (MQW) can be changed. These modifications of the absorption spectra due to electric field also effect the refractive index of the material through the Kramers-Kronig relation. Also the interaction of the electrons and holes with the optical field contributes the refractive index change named as the *plasma* contribution. According to the Drude model, the change in the carrier population induce the refractive index change as follows,

$$\Delta n \approx \frac{-N_x e^2 \lambda^2}{8\pi^2 \epsilon_0 n c^2 m_x^*},$$

where N_x and m_x^* are the excitonic (i.e., electron-hole) concentration and the excitonic effective masses, respectively [17]. Empirically, for a density of 10^{19} cm^{-3} in electron-hole doping for fused silica at a wavelength 1.55 μm, we are expecting a change in the refractive index $\Delta n \sim 0.0149$. The refractive index of fused-silica for the given wavelength is $n = 1.444$. So plasma effect has a non-negligible of a per cent contribution to the refractive index change.

2.4 Quantum Confined Stark Effect

As it is known, the applied electric field causes a change in both wave function and energy state of the quantum systems. The perturbation theory predicts a shift in the ground energy called *Stark effect* that triggers the excitation of the electrons from valence band to the conduction band. The quantum structures

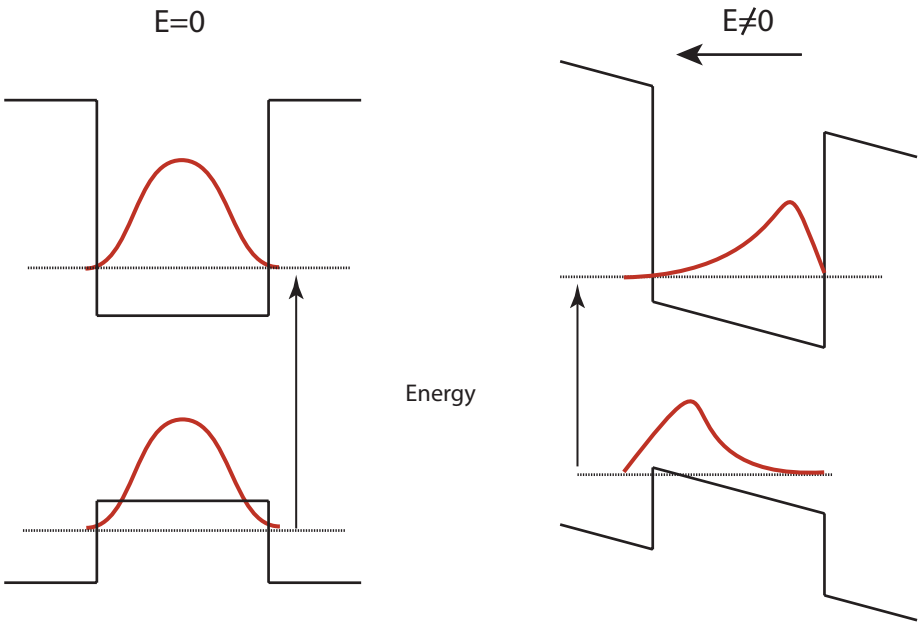

Figure 2.2: In the presence of the electric field, band gap of the material is reduced which enables in tunnelling of the electron to the conduction band.

involve alternating layers of GaAs and AlGaAs with a thickness of the order of 100 nm. These layers form the quantum wells where each well shows quantum mechanical size effects. Applied electric field perturbs the states and pushes them to get closer. As a result the exciton resonances shift to lower photon energies, in other words longer wavelengths, hence introduces a *red shift*. This red shift results with the new absorption peaks associated with the formation of the exciton and enables forbidden transitions. In these structures, the separation of the excited electron with the hole is expected to be larger than the thickness of the layer, however the thin well walls of the structure impose a constrain to the exciton structures to bring them closer.

This constrain restrict the movement of the exciton and this restriction is called quantum confinement. The benefit of the confinement systems is the associated absorption peaks which would otherwise not be easily observed in the bulk systems [18]. Although the electric field brings the states closer, it applies force on electrons and holes in opposite directions which weakens the binding of the exciton. But we can still observe well defined excitonic states. Compared to the bulk systems, under such higher electric fields, exciton resonances can be remain in the confinement systems without excessive broadening [27]. By choosing the appropriate frequency of the light for the applied electric field, the absorption of the electro-optic medium can be changed which is the basis of an optical modulator [18]. The application of this effect to the bulk systems can be questioned. The following reason may answer this question. The contribution of the electric field is taken as a perturbation to the solution of the eigenstates of the system. To get significant shift in the eigenstates of the system, the electric field energy eEa_B in terms of the effective Bohr radius, electron charge and electric field should be comparable with the absorption edge energy, $eEa_B \geq \Delta$. This equation needs a field of the order of 10^6 V/m for different material parameters. However such strong fields of this order broaden even destroy the exciton resonances. One of the reason beside this broadening is the field ionization of the exciton, penetration of the electron through the finite Coulomb barrier at finite fields. The other reason is the impact ionization. Free carriers in the medium can gain high energies in the presence of electric field. The hitting of this high energetic carriers to the exciton may result with ionization of the exciton or broadening of the excitonic resonance [19]. By confining the electron-hole system, one can overcome this problem for the following reasons:

- since the electrons and holes have opposite electric charges, in the presence of the electric field they feel repulsive electric force. This force pushes them to opposite sides of the layers that reduce the energy of the electron-hole pair resulting with a red shift.
- the walls of the quantum well prevent the electron and hole from tunnelling out of the layers. For the strong confinement, it is important that, the well width should be narrow compared to the exciton size [27].

Stark effect modifies the excitonic resonances and this modification yields change in the refractive index through the Kramers-Kronig relation. As a result we can achieve Pockels or Kerr like effect to modulate the light.

2.5 Franz-Keldysh Effect

In the previous section, the effect of the applied electric field on the quantum systems is expressed as Stark effect. Reduction of the band gap by the Stark effect results in the increasing excitation of the electrons to the conduction band with the energy $\hbar\omega < E_g$. However this work for the quantum confined systems. Because, if the applied field exceeds the classical ionization energy of the order of a few times, exciton resonance broadens as a result of ionization [27] as mentioned in the previous section. For the bulk semiconductors, Franz and Keldysh independently proposed another effect of the electric field. The applied field results in an exponential tail of the wave functions into the forbidden zone of the semiconductor, and over this tail electrons can tunnel to the conduction band from the valence band absorbing a photon with a energy $\hbar\omega < E_g$ [29]. As a result, overlap between the hole and electron wave functions leads the transition for the energies smaller than E_g. As the electric field increases, the exponential tail and amplitudes of the Franz-Keldysh oscillation increases [28].

Fascinating property of the Franz-Keldysh effect is that it renders a single semiconductor to have an tunable "band gap". Recall that Stark effect is observed in quantum wells which requires expensive fabrication techniques. In contrast to the Stark effect, Franz-Keldysh effect lets us use bulk semiconductors which has a simple growth procedure covering a wide range of the wavelengths. Also insensitivity to the high optical powers make this approach stable. Powers higher than 250 W/cm^2 saturates the Stark effect, on the other hand the Franz-Keldysh effect remains unperturbed up to powers of 20 kW/cm^2. Above this power an other optical effect named band filling contributes. Response time of the electro-optic devices are limited by the low saturation intensity which means that higher intensity results with higher response speed. For the optical modulators this

property becomes important for the following reasons:

- optical power as low as mW can saturate the excitons which will diminish the Stark effect,
- to modulate the light by using the Stark effect we need polarization preserving waveguides.

Although it seems that the usage of the Franz-Keldysh effect is advantageous compared to the Stark effect, huge power need of the system must also be considered [20].

2.6 Quantum Confined Pockels Effect

For the case of quantum wells, if the barrier and well materials share common ion such as $In_xGa_{1-x}As$-InP at interfaces, the sample shows optically isotropic medium in the plane perpendicular to the growth direction. Under applied electric field, this rotational symmetry at the interface is broken and a strong enhancement of quantum confined Pockel effect is observed. Theoretical background of this symmetry breakdown can be understood by adding an interface term to the valence band Hamiltonian. This term is invariant of the C_{2v} group and can be treated as a perturbation in the framework of the classical envelope-function theory. In other words, because of this perturbation, heavy and light hole states are mixed as a function of applied field at the minizone, and this mixing breaks the in-plane isotropy [22].

2.7 Burstein-Moss Effect

In 1953, Tanenbaum and Briggs tried to explain the different band gap measurements of indium antimonide (InSb) for different temperatures. There are divergent band gap values with the increasing temperature and they concluded

that this results from impurity effects [1]. However this anomalous change in the absorption edge is explained differently in the same year by Burstein and Moss independently. They proposed that the explanation of this absorption limit is based on the small effective mass of electrons rather than impurity effect. Since the bottom of the conduction band of InSb has sharp curvature and at this region there exists small density of states. This density of states results with small effective mass of electrons. As the carrier density increases the difference between the Fermi energy level E_F and the conduction band edge increases rapidly since the electrons fill the small available states in the conduction band [2]. For the case of

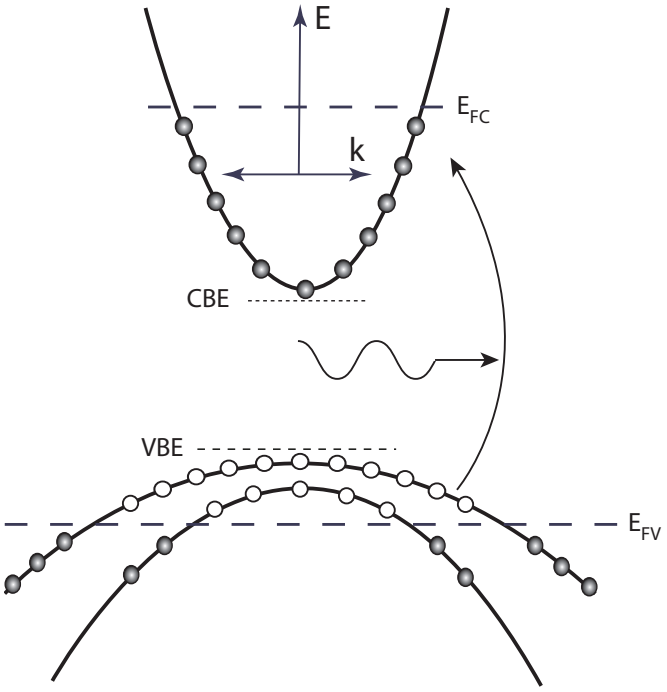

Figure 2.3: As the carrier densities increase in both valence band and conduction band, excitation of an electron to the conduction band requires more energy.

n-type doping, the electron contribution to the conduction band comes from two different type of sources. One of the sources is the electrical injection of donors to the semiconductor. The thermal ionization of the donors introduces electrons to the conduction band. The other means is by photo-injection excitation of an electron from valence band to the conduction band, absorbing a photon. As the free carrier concentration increases in the medium they fill the available states

at the bottom of the conduction band. So the excitation of an electron over the Fermi level of the conduction band while conserving its momentum (with the same k value) requires much more energy compared to the band gap E_g of the intrinsic semiconductor as shown in Fig. 2.3 However, due to the many body effects, for high densities, band gap narrowing effect can be also observed [23] as stated in the following Fig. 2.4. More about the band gap renormalization will be given in the following chapters.

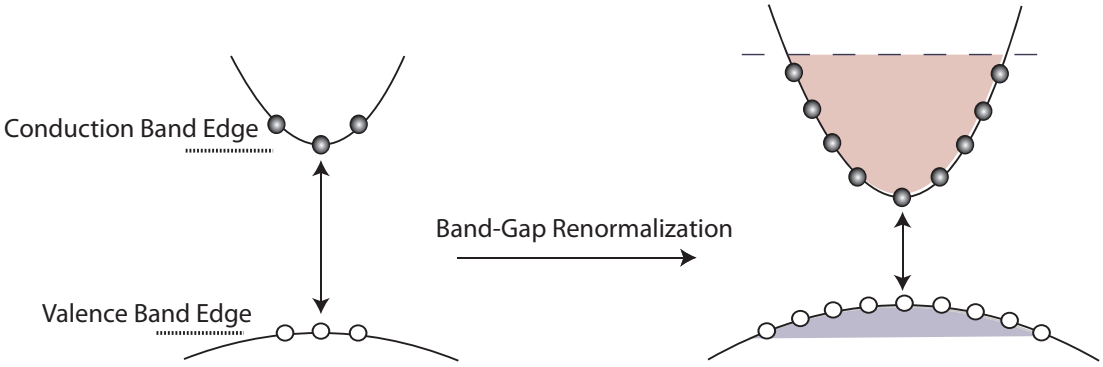

Figure 2.4: As the carrier densities increase in both valence band and conduction band, due to the many body effects band gap is renormalized.

2.8 Purcell Effect

Finally, we would like to discuss an effect which is not an electro-optic or electro-absorption effect, but nevertheless it has recently attracted strong interest in a similar context. The main physical idea in this effect is the control of the spontaneous emission. One of the main phenomena for the creation of light is spontaneous emission. In the presence of stimulated emission, spontaneous emission can be somehow troublesome. Since it can limit the performance of photonic devices such as lasers, displays, illuminations and so on. For lasers, stimulated light is coherent, however spontaneous emission (SE) does not contribute to lasing. Since it does not couple with the laser beam it emerges as noise that is an unwanted

situation that scientists want to get rid of. Also for the case of the LEDs, the problem emerges in a different way. Basic working principle of the LEDs is based on the SE. However, the problem lies under this idea is the only limited ratio of the light extracted from the device and most of the light is confined inside the semiconductor. For different situations there are different motivations to inhibit the SE or to increase the efficiency of SE [24].

By using a cavity, Purcell suggested a method to control the SE rate. Usage of a cavity leads to a modification of dipole-photon coupling and available photon modes allow us to fabricate high efficiency LEDs also let us to inhibit the undesired wavelengths [25].

Now let us first analyse the the working principle of Purcell effect. An emitter with a wavelength λ_e, linewidth $\Delta\lambda_e$ placed in a resonance which has a single mode with a wavelength λ_c, linewidth $\Delta\lambda_c$ and a quality factor $Q = \lambda_c/\Delta\lambda_c$. Since $\lambda_e \ll \Delta\lambda_c$, the time need for photon to leave the cavity is much shorter than the radiative lifetime. So the re-absorption of the emitted light is now negligible which can be defined as weak coupling regime. Different from the vacuum the emitter feels a quasi-continuum of modes. By using the Fermi golden rule, the rate of spontaneous emission is written as

$$\frac{1}{\tau} = \frac{4\pi}{\hbar}\rho_{cav}(\omega \left\langle |\vec{d}\cdot\vec{\epsilon}(r)|^2 \right\rangle,$$

where $\vec{\epsilon}(r)$ is the vacuum electric-field vector at the location (r) of the emitter and $\vec{d}$ is the electric dipole, $\rho_{cav}(\omega)$ is the density of modes of the cavity at the emitters frequency. SE rate in the cavity mode, compared to the total SE rate in a medium, is given by the Purcell factor

$$F_p = \frac{3Q\lambda_c^3}{4\pi^2 n^3 V},$$

where n is the refractive index of the medium, Q is the quality factor of the cavity and V is the volume of the cavity [26]. As a result, the cavity increase the spontaneous emission of the dipole by tuning the frequency of the emitter.

Chapter 3

The Relevance of This Work to Semiconductor Lasers

On 6 August 1960, Theodere Mainman published a paper in *Nature*, about the first working laser developed at the Hughes Research Laboratory in California [46]. He pumped silver coated ruby rod with high power flash lamp and the laser produced a short of flash light. This marked the initiation of a research area which turns into a billion dollars worth of industry. By the development of different types of laser such as semiconductor lasers, solid state lasers, gas lasers, etc, lasers inevitably became part of our lives. If we take into account the economic impacts of the lasers, the semiconductor lasers stand out. They are now widely used in areas such as CD players, laser printers, military and bio-medical applications. Continuously improvement in the performance of the semiconductor lasers such as low-threshold current, high speed direct current modulation, ultra-short optical pulse generation, high optical output power, low cost and etc. is the main reason behind this major surge [47].

3.1 Basic Structure

The working principle of a semiconductor laser basically depends on the recombination of the carriers injected from the $p-n$ junction. Basic schematic of an semiconductor laser is shown in Fig. 3.1. When we forward bias the junction, electrons are injected from the n-type doped layer and holes are injected from the p-type doped layer to the intrinsic (active) region. After the accumulation of the electrons and the holes in the active region (pumping), electrons and holes are stimulated to recombine in the active region. Each stimulated electron-hole recombination results in the emission of a coherent light to the optical field.

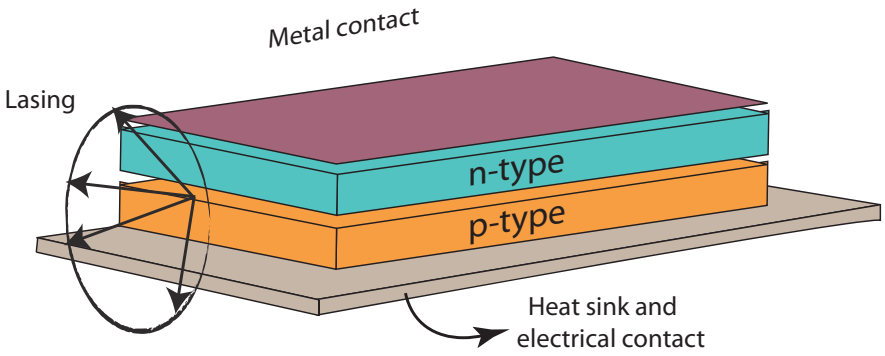

Figure 3.1: Basic structure for the semiconductor laser.

3.2 Photoexcitation and Attainment of Quasi-Equilibrium

The primary purpose of this thesis is to study the refractive index change due to equal concentration of electron and holes ($n = p$). This can be achieved by

the basic p-n junction drawn in Fig. 3.1 through electrical injection. However,

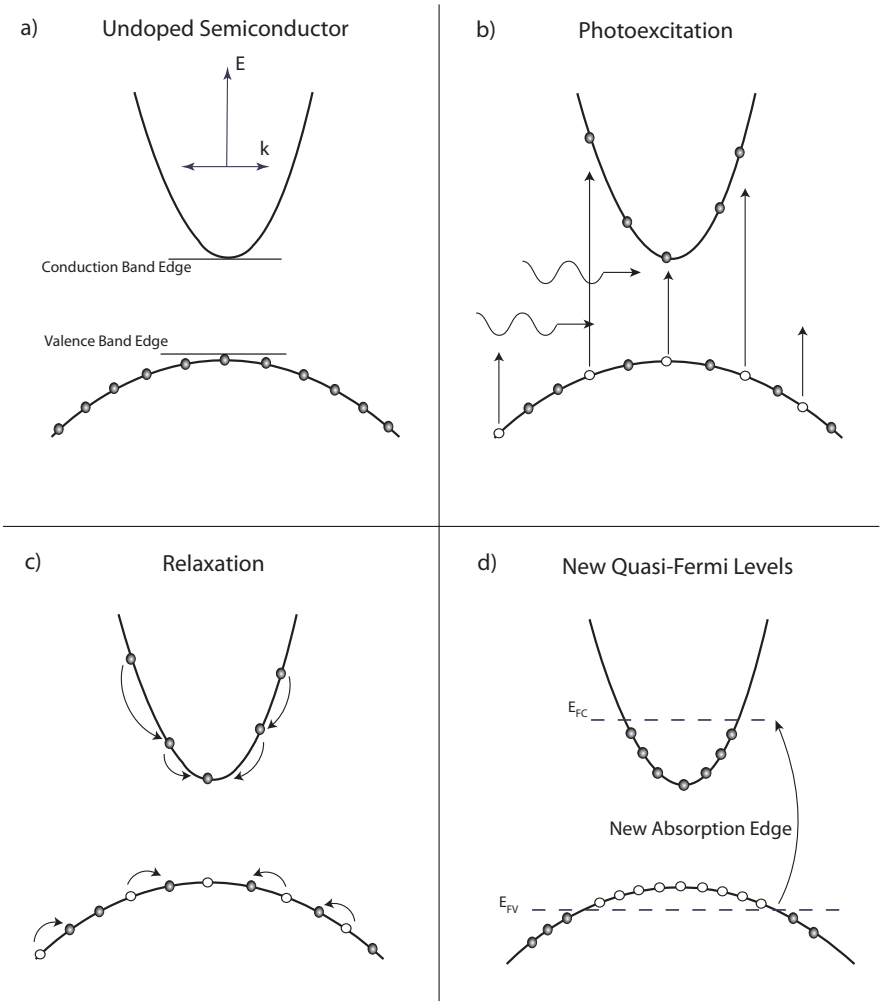

Figure 3.2: Photoexcitation in semiconductor lasers.

in the case of InN, its p-doping is a major challenge. For this reason, we shall consider optical injection of equal number of electron and holes. In Fig. 3.2(b) we show the electron hole generation under a broadband illumination with an energy highly above the band gap of InN. The carriers then quickly relax to band edges Fig. 3.2(c) by emitting optical phonons. This results in the attainment of a new quasi-equilibrium of the excited carriers (see Fig. 3.2(d)). It should be noted that these electron-hole pairs will radiatively recombine in a duration of nanoseconds and this non-equilibrium population will be lost. For this reason the

optical pumping process needs to be kept on, in order to preserve a steady-state quasi-equilibrium carrier distribution.

3.3 Carrier Distribution

This quasi-equilibrium carrier distribution corresponds to the population inversion which is required so as to amplify an optical radiation of a frequency ν. The quasi-Fermi energy difference between the electrons and the holes determines the photon energy. Note that, under equilibrium, Fermi levels of electrons E_{Fc} and Fermi level for the holes E_{Fv} equal to the Fermi level of the whole system

$$E_{Fc} = F_{Fv} = E_F.$$

However, under optical or electrical injection, the system is driven into non-equilibrium state. The Fermi levels of the electrons and the holes split and construct the new quasi Fermi levels of the systems. Under non-equilibrium conditions, the electron concentration n and the hole concentration p are given as

$$n = N_c \exp\left(-\frac{E_c - E_{Fc}}{k_B T}\right),$$

$$p = N_v \exp\left(-\frac{E_{Fv} - E_v}{k_B T}\right).$$

Here, under parabolic band assumption the effective density of states for the electrons N_c and that for the holes N_v are written as,

$$N_c = 2\left(\frac{2\pi m_e^* k_B T}{h^2}\right)^{3/2},$$

$$N_v = 2\left(\frac{2\pi m_h^* k_B T}{h^2}\right)^{3/2},$$

where k_B is the Boltzmann constant and h is Planck's constant.

The new quasi-Fermi levels become,

$$E_{Fc} = E_c + k_B T \ln\left(\frac{n}{N_c}\right),$$

$$E_{Fv} = E_v - k_B T \ln\left(\frac{p}{N_v}\right),$$

where E_c is the bottom energy level of the conduction band and E_v is the top of the valence band.

The distribution function for the electrons having energy E_1 in the valence band is f_1 and for the electrons having energy E_2 in the conduction band is f_2. By using the quasi-Fermi levels E_{Fc} and E_{Fv}, we can write f_1 and f_2 as

$$f_1 = \frac{1}{\exp\left[(E_1 - E_{Fv})/k_B T\right] + 1},$$

$$f_2 = \frac{1}{\exp\left[(E_2 - E_{Fc})/k_B T\right] + 1}.$$

f_1 is given for the occupation of electrons for the valence bands, so the hole distribution function in the valence band is given by [1-f_1] [49].

3.4 Chirp

Up to this point, we assume that the semiconductor laser is very stable and lases at a single mode. However, during population inversion, the accumulation of electrons and holes in the active region changes the absorption coefficient of the semiconductor. Also the new carrier population renormalizes the band gap.

When an electromagnetic pulse propagates through a medium, the bound electrons of the dielectric display a wavelength dependent response. In general, the refractive index of the material varies as

$$1 < n_{red}(\lambda) < n_{yellow}(\lambda) < n_{blue}(\lambda).$$

The variation of the refractive index results in different group velocities of each spectral component as

$$v_g(\lambda) = \frac{c}{n_\lambda},$$

where c is the speed of light. This phenomenon is named as dispersion. Longer wavelength component of the pulse has larger group velocity, therefore leading part of the pulse has low frequency which is called red shifted. However, if the

medium has an anomalously dispersive property so that refractive index changes as

$$1 < n_{blue}(\lambda) < n_{yellow}(\lambda) < n_{red}(\lambda),$$

the leading part of the pulse is now high frequency components which is called blue shifted. As a result of the dispersion, the instantaneous frequency of the pulse changes and this change is called *chirp*. Also nonlinearities in the medium causes chirp on the pulse. Besides, dispersion and nonlinearities, in semiconductor lasers refractive index change depending on electron and hole population leads to a chirp which is the main subject matter of this thesis. In this context, we can distinguish between two different types of chirp. If the instantaneous frequency has an increasing function, we call it *up-chirped* pulse. Fig. 3.3 shows the difference of these types of chirp. In this type, the leading part of the pulse is blue shifted. On the other hand, if the pulse has time dependent decreasing instantaneous frequency, it is called *down-chirped* pulse and the leading part of the pulse is red shifted. The chirp on the pulse can be removed by propagating the wave in a suitable dispersive medium.

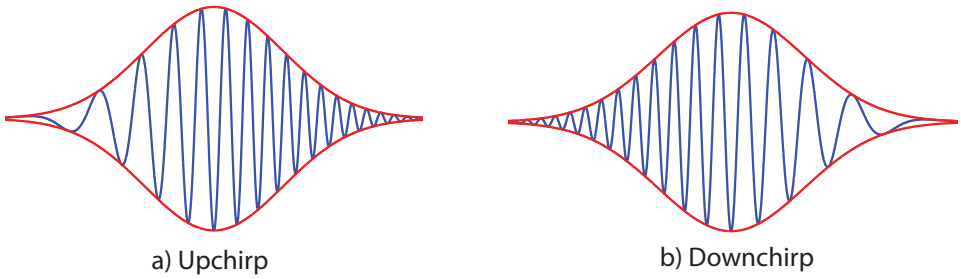

Figure 3.3: (a) shows the up-chirp with increasing instantaneous frequency, (b) shows the down-chirp with decreasing instantaneous frequency.

Chapter 4

Further Technical Preliminaries

In this chapter, we provide in depth information on three technical issues which will be of importance in the rest of the thesis. These are the tetrahedron integration technique by Lehmann Taut and the discussion of Van Hove singularities in bulk semiconductors. The common denominator of the both subjects is that they both take place in the reciprocal lattice. Finally, we provide some theoretical information on the Kramers-Kronig relations.

4.1 Brillouin-Zone Integrations

Quite commonly in solid state calculations, one ends up with an integration over a surface (usually Fermi surface), as in density of states, effective mass tensor or response functions. Conventional integration routines for calculating the density of states and similar kind of integral types in the form

$$\int \frac{dS}{|grad\Delta\varepsilon(\mathbf{k})|} A(\mathbf{k}),$$

encounter serious complications. In an energy interval, $D(\varepsilon)$ is inversely proportional to the square root of the mesh points and increasing in the mesh point leads to increase of statistical noise. As a result, Gilat and Raubenheimer propose a

different integration routine to solve this problem [40]. They divided whole Brillioun zone into *cubes* with the same volume. All the reciprocal space is reached by linear extrapolation of the cube centers. The integration over the constant energy or frequency surface is now replaced by the cross sections of small areas between the cubes and the constant surfaces. On the other hand, Lipton and Jacobs modified this method, and they interpolated the energy points between the corners of the cubes that reduces the computational load [41]. However, both of these methods cannot fill the boundary of the reciprocal spaces so these boundaries need to be coded explicitly.

4.1.1 Lehmann-Taut Method

Lehmann and Taut approached to the problem in a different way and they divided reciprocal lattice into *tetrahedra*, as the whole Brillioun zone can be totally divided into tetrahedra including the boundaries [42]; see Fig. 4.1.

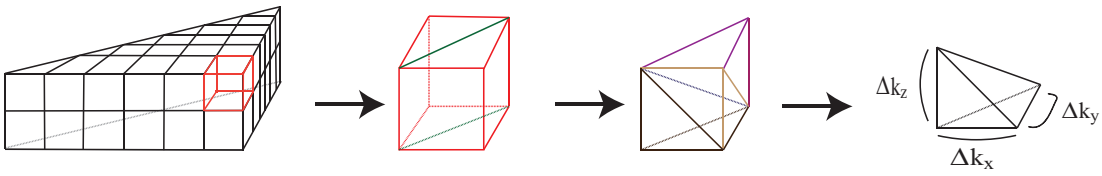

Figure 4.1: Filling of Brillioun zone with tetrahedra.

Wurtzite InN has hexagonal reciprocal structure. Any volume integration over this Brillioun zone can be reduced to *irreducible Brillioun zone* (IBZ) by using the all symmetries of the lattice as shown in Fig 4.2.

Then the IBZ is divided into a mesh of 40×40×40 in both basal plane and along the z axis shown in Fig. 4.3 and every mesh is then divided into tetrahedra. Let the energy value at $k_0 = 0$ corner of the tetrahedron be $\Delta\varepsilon_0$ and for the corners $k_i (i = 1, 2, 3)$ be denoted as $\Delta\varepsilon_i$, respectively. Within the tetrahedron, the energy values $\Delta\varepsilon(\mathbf{k})$ can be determined by linear interpolation as

$$\Delta\varepsilon(\mathbf{k}) = \Delta\varepsilon_0 + \mathbf{b} \cdot \mathbf{k}.$$

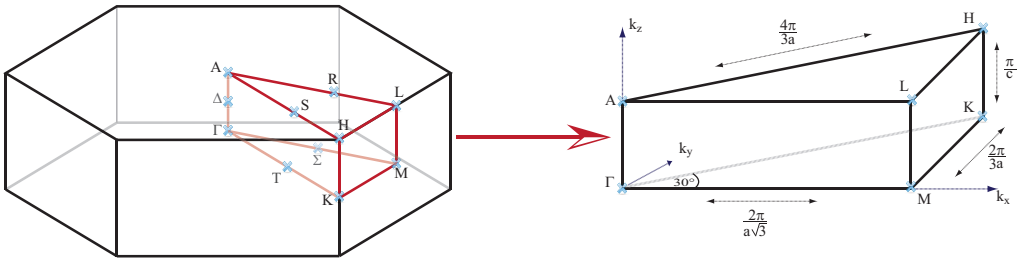

Figure 4.2: First Brillioun zone of the wurtzite lattice and its IBZ

b is determined by these series of formulas,

$$\mathbf{r_j} \cdot \mathbf{k_i} = \delta_{ij}; \quad \mathbf{r_1} = \frac{\mathbf{k_2} \times \mathbf{k_3}}{v}; \quad \mathbf{r_2} = \frac{\mathbf{k_3} \times \mathbf{k_1}}{v}; \quad \mathbf{r_1} = \frac{\mathbf{k_1} \times \mathbf{k_2}}{v},$$

and

$$\mathbf{b} = \sum_{i=1}^{3} (\Delta\varepsilon_i - \varepsilon_0)\, \mathbf{r}_i$$

where v is the six times tetrahedron volume. Also the function $A(\mathbf{k})$ is interpolated in a similar way as

$$a(\mathbf{k}) = a_0 + \mathbf{a} \cdot \mathbf{k}.$$

Now we knit the any kind of the integrand as a spider's net.

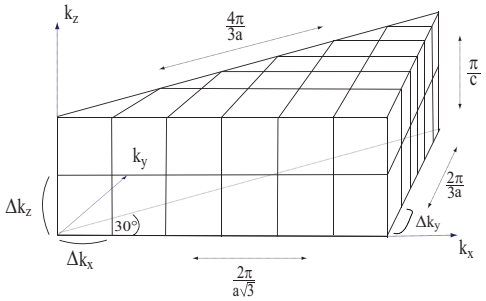

Figure 4.3: Meshing on the IBZ

4.1.2 Application to Density of States

The density of states is given by the expression,

$$g(E) = \int \frac{dS}{grad\Delta\varepsilon(\mathbf{k})},$$

dS represents the surface integral over the volume. By a simple derivative, the denominator turns into form

$$grad\Delta\varepsilon(\mathbf{k}) = grad(\Delta\varepsilon_0 + \mathbf{b}\cdot\mathbf{k}) = \mathbf{k},$$

since $grad\Delta\varepsilon_0 = 0$. The contribution of one tetrahedron to the density of states is calculated with an energy $\Delta\varepsilon(k) = \varepsilon$ is

$$i_0(\varepsilon) = \int_{\Delta\varepsilon(k)=\varepsilon} \frac{dS}{b},$$

and this integral representation turns into simple mathematics calculation such as

$$i_0(\varepsilon) = f(\varepsilon).|b|^{-1}.$$

$f(\varepsilon)$ is the intersection of the constant energy surface with the tetrahedron and these cross sections shown in Fig. 4.4 can be written as the sum of the triangular areas [42].

$$f(\varepsilon) = \begin{cases} f_0 & \Delta\varepsilon_0 \leq \Delta\varepsilon \leq \Delta\varepsilon_1 \\ f_0 - f_1 \quad \text{for} & \Delta\varepsilon_1 \leq \Delta\varepsilon \leq \Delta\varepsilon_2 \\ f_3 & \Delta\varepsilon_2 \leq \Delta\varepsilon \leq \Delta\varepsilon_3 \end{cases}$$

where the integrands come out as,

$$f_0|\mathbf{b}|^{-1} = \frac{v}{2}\frac{(\varepsilon-\Delta\varepsilon_0)^2}{(\Delta\varepsilon_1-\Delta\varepsilon_0)(\Delta\varepsilon_2-\Delta\varepsilon_0)(\Delta\varepsilon_3-\Delta\varepsilon_0)}$$

$$f_1|\mathbf{b}|^{-1} = \frac{v}{2}\frac{(\varepsilon-\Delta\varepsilon_1)^2}{(\Delta\varepsilon_1-\Delta\varepsilon_0)(\Delta\varepsilon_2-\Delta\varepsilon_0)(\Delta\varepsilon_3-\Delta\varepsilon_0)}$$

$$f_3|\mathbf{b}|^{-1} = \frac{v}{2}\frac{(\varepsilon-\Delta\varepsilon_3)^2}{(\Delta\varepsilon_1-\Delta\varepsilon_0)(\Delta\varepsilon_2-\Delta\varepsilon_0)(\Delta\varepsilon_3-\Delta\varepsilon_0)}.$$

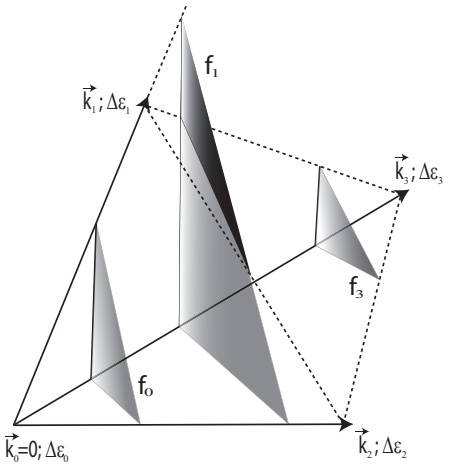

Figure 4.4: Different intersections of a tetrahedron with three different constant energy surfaces.

4.1.3 Effective Mass and Dielectric Tensors

In this thesis we need the energy-dependent effective masses. To obtain the m^*(E), we can define the group velocity of the carrier as

$$v = \frac{1}{\hbar}\nabla_k E.$$

By taking the derivative of the velocity, we get the acceleration,

$$\begin{aligned} \mathbf{a} &= \frac{d\mathbf{v}}{dt} &&= \frac{1}{\hbar}\frac{d}{dt}\nabla_k E \\ &&&= \frac{1}{\hbar}\nabla_k \left[\nabla_k E \cdot \frac{d\mathbf{k}}{dt}\right] \end{aligned} .$$

The acceleration of the free carrier is a result of an external field $\mathbf{F}$ and time dependent wave solution of the carrier requires

$$\mathbf{F} = -\hbar(d\mathbf{k}/dt).$$

When we substitute $\mathbf{F}$ into the $\mathbf{a}$ and from $\mathbf{F} = m^*a$,

$$\mathbf{a} = -\frac{1}{\hbar^2}\nabla_k \nabla_k E \cdot \mathbf{F},$$

$$m^* = \frac{\hbar^2}{\partial^2 E/\partial k^2},$$

we get the energy-dependent effective mass of the carrier [43].

Just like the density of states and energy-dependent effective mass tensor calculations, we can obtain the imaginary part of the dielectric function using the tetrahedron integration technique [50]. The corresponding expression is given by

$$Im\left\{\epsilon^{ab}(\omega)\right\} = \frac{e^2}{\pi}\sum_{v,c}\int_{BZ} d\mathbf{k}\,\mathbf{r}^a_{vc}(\mathbf{k})\mathbf{r}^b_{vc}(\mathbf{k})\mathbf{r}^a_{vc}(\mathbf{k})\delta\left(E_c(\mathbf{k}) - E_v(\mathbf{k}) - \hbar\omega\right).$$

4.2 Van Hove Singularities

We have shown the calculation method of density of states by using Lehmann-Taut method for the type of integral

$$g_n(\varepsilon) = \int_{S(\varepsilon)} \frac{dS}{\nabla_{\mathbf{k}}\varepsilon_n(\mathbf{k})},$$

which reconciles the density states with the band structure of the semiconductor. More detailed work is shown in the preceding chapters. At this point, we prefer to focus on the mathematical meaning. The $S(\varepsilon)$ represents a constant energy surface. If we use for the energy, that of the energy difference between bands n and n' as in

$$\varepsilon_n(\mathbf{k}) - \varepsilon_{n'}(\mathbf{k}) = \varepsilon_0,$$

and similarly for the gradient

$$\nabla\left[\varepsilon_n(\mathbf{k}) - \varepsilon_{n'}(\mathbf{k})\right] = 0,$$

what we obtain is called joint density of states since it gives the density of pair of states: one is empty, the other one is occupied with an energy difference ε_0. Hence the joint density of states is represented as [44]

$$J_{nn'} = \int_{\varepsilon_n(\mathbf{k})-\varepsilon_{n'}(\mathbf{k})=\varepsilon_0} \frac{dS}{\nabla\left[\varepsilon_n(\mathbf{k}) - \varepsilon_{n'}(\mathbf{k})\right]}.$$

The singularities in the integrand are known as *Van Hove singularities* and occur when the constant energy surface contains the band points whose gradient vanishes. However, these singularities are integrable and yields finite values and contribute to the density of states and the slope of the density of states at these

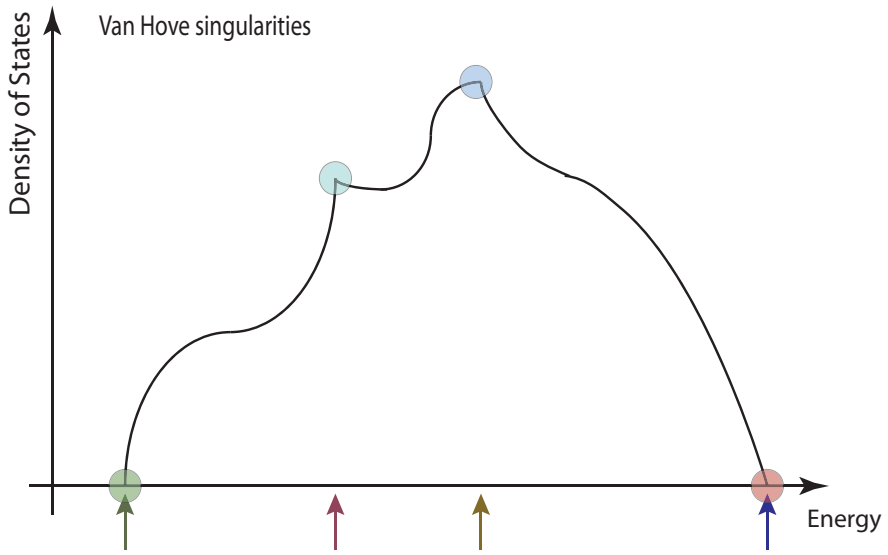

Figure 4.5: Different types of van Hove singularities. The arrows indicate the energies where the singularities exist. The circles shows the discontinuities in the derivative of the density of states .

point diverges [45]. A basic schematic of these singularities in the density of states is shown in Fig. 4.5.

We can encounter these singularities when,

$$\nabla_{\mathbf{k}}\varepsilon_n(\mathbf{k}) = \nabla_{\mathbf{k}}\varepsilon_{n'}(\mathbf{k}) = 0,$$

or more generally for

$$\nabla_{\mathbf{k}}\left[\varepsilon_n(\mathbf{k}) - \varepsilon_{n'}(\mathbf{k})\right] = 0.$$

The first condition occur at the high symmetry points and the second condition may occur at any $\mathbf{k}$ vector [44].

Now lets go back the physical meaning and importance of these singularities. For the direct transitions between bands n and n' which are parallel at a particular $\mathbf{k}$ values with an energy difference $\varepsilon_{nn'}$, a different density of states is responsible [52]. At these points during measurement of the optical properties of semiconductor, a peak is expected. For our cases, computation of the absorption of the medium for the photons with an energy $\hbar\omega_{nn'} = \varepsilon_{nn'}$ we are also expecting

peaks in the corresponding energies of these singularities. For the calculation of the imaginary part of the dielectric function at these energies and in their neighbourhood, van Hove singularities dominate the absorption characteristics of the semiconductor.

4.3 Kramers-Kronig Relation

As a main idea of this chapter we almost gave the technical procedure for our computational work. As a final step we need to calculate the imaginary and real part of the dielectric function to conclude the refractive index change for the InN. Imaginary part of the dielectric function is responsible for the absorption of the medium and again is stated by the following formula

$$Im\left\{\epsilon^{ab}(\omega)\right\} = \frac{e^2}{\pi}\sum_{v,c}\int_{BZ} d\mathbf{k}\,\mathbf{r}^a_{vc}(\mathbf{k})\mathbf{r}^b_{vc}(\mathbf{k})\mathbf{r}^a_{vc}(\mathbf{k})\delta\left(E_c(\mathbf{k}) - E_v(\mathbf{k}) - \hbar\omega\right).$$

To compute the real part of the function by using the imaginary part we use the causality principle and the mathematical procedure is given by the *Kramers-Kronig* relation. So at this point it is necessary to open a parenthesis to discuss the Kramers-Kronig relations. These details are taken from the reference [52]. These relations have great importance since they allow us to evaluate the components of the dielectric function, conductivity, susceptibility or other optical properties of the semiconductor, if we know the one of reflection or absorption of the medium. By involving the causality, derivation between the complex and real part of the response function can be done. To describe the linear response $\hat{X}$ of the system for an arbitrary time t and a position $\mathbf{r}$ to a external perturbation in terms of an external stimulus $\hat{f}$ at a time t' and location $\mathbf{r}'$ we use the following formula

$$\hat{X}(\mathbf{r}), t = \int\int_{\infty}^{\infty} \hat{G}(\mathbf{r}, \mathbf{r}', t, t')\hat{f}(\mathbf{r}', t')d\mathbf{r}'dt',$$

where $\hat{G}(\mathbf{r}, \mathbf{r}', t, t')$ is the response function. By using the Cauchy's theorem and causality we get the relation

$$\hat{G} = \frac{1}{i\pi}P\int_{\infty}^{\infty}\frac{\hat{G}(\omega')}{\omega' - \omega}d\omega'.$$

When we divide $\hat{G}$ into real and imaginary parts as

$$\hat{G} = G_1(\omega) + iG_2(\omega),$$

and this leads the following relations between the real and imaginary parts of $\hat{G}$

$$G_1(\omega) = \frac{1}{\pi} P \int_{\infty}^{\infty} \frac{G_2(\omega')}{\omega' - \omega},$$

$$G_2(\omega) = -\frac{1}{\pi} P \int_{\infty}^{\infty} \frac{G_1(\omega')}{\omega' - \omega}.$$

For the real part of the dielectric function, the expression is stated in Gaussian units as

$$Re\left\{\epsilon(\omega)\right\} = 1 + \frac{2}{\pi} P \int_{0}^{\infty} \frac{\omega' Im\left\{\epsilon(\omega')\right\}}{\omega'^2 - \omega^2} d\omega'.$$

More information and intermediate steps can be found in the relevant chapter of the Ref. [52].

Chapter 5

Band Gap Renormalization

Since the invention of the first semiconductor laser, the understanding of the density dependent optical spectra has attracted attention. Especially many-body effects of highly dense carriers such as exchange and correlation energy in the material renormalize the band gap and also affect other optical properties such as refractive index and the overall optical susceptibility. The spin distribution of the carriers ultimately affect the charge distribution of the system. Pauli principle excludes the same spin electrons or holes to be in the same position at the same time. As a result, electrostatic energy of the system will be reduced according to the redistribution of the carriers and the energy difference compared to noninteracting uniformly distributed carriers is called *exchange energy* [30]. However, this energy deviates from the exact non-relativistic energy of the system. The difference between these energy is called *correlation energy*. This Hartree-Fock energy is an upper bound limit to the non-relativistic exact energy of the system, which means that the correlation energy is always negative [31].

Increasing in the carrier population strongly influences the Coulomb interaction between the electron-hole (e-h) pairs. In the plasmas, one emerging property is the screening of the Coulomb potential, and the (e-h) plasma screening of the Coulomb interaction is given by,

$$V_s(\mathbf{q}, w) = V_q/\varepsilon(\mathbf{q}, w),$$

where V_q is the unscreened Coulomb potential and the $\varepsilon(\mathbf{q}, w)$ is the longitudinal dielectric function. The dielectric function is usually approximated by Lindhard formula [33].

$$\varepsilon(\mathbf{q}, w) = 1 - V_q \frac{1}{V} \sum_{i=e,h;k} \frac{f_{i,\mathbf{k}} - f_{i,\mathbf{k}+q}}{\hbar\omega + i\delta - \varepsilon_{i,\mathbf{k}+q}},$$

where $\varepsilon_{i,\mathbf{k}}$ and $f_{i,\mathbf{k}}$ are the e-h energies and distribution functions respectively. The subscripts i and k refer to the band index and wave vectors respectively. If the carriers are in the equilibrium state, the distribution function is given by the Fermi distribution

$$f_{i,\mathbf{k}} = \frac{1}{\exp\left[(\varepsilon_{i,\mathbf{k}} - \mu_i)\beta\right] + 1},$$

where μ_i is the chemical potential, $\beta = 1/k_b T$.

5.1 Plasmon-Pole Approximation

In 1989 Haug and Koch simplified the Coulomb self-energy calculation by using the so called plasmon-pole approximation [32]. By using static plasmon-pole approximation, Lindhard formulation turns into the following simple form,

$$\frac{1}{\epsilon_{\mathbf{q}}} = \left[1 - \frac{\omega_{pl}^2}{\omega_q^2}\right],$$

where ω_q is the dispersion of the effective plasmon mode and for 3D systems. The governing formulas can be written as

$$V_q = \frac{4\pi e^2}{\epsilon_0 q^2},$$

$$\omega_{pl}^2 = \frac{4\pi e^2 n}{\epsilon_0 \mu_x} = \left[\frac{E_0}{\hbar}\right]^2,$$

$$\omega_q^2 = \omega_{pl}^2 \left[1 + \frac{q^2}{\kappa^2}\right] + \frac{C}{4}\left[\frac{\hbar q^2}{2\mu_x}\right]^2,$$

where μ_x is the reduced $e-h$ mass $\mu_x = m_e m_h/(m_e + m_h)$, n is the plasma density, C is a numerical constant, E_0 is the Rydberg constant and κ is the inverse screening length, which can be obtained by the formula

$$\kappa^2 = \frac{4\pi e^2}{\epsilon_0} \sum_i \frac{\partial n}{\partial \mu_i}.$$

The band gap of the material shrinks with the increasing carrier population due to the many-body exchange and correlation effects. The corresponding the band gap shift is given by

$$\begin{aligned}\Delta E_g &= [V_s(\mathbf{r}=0) - V(\mathbf{r}=0)] - \tfrac{1}{V}\textstyle\sum_{\mathbf{q}} V_s(\mathbf{q})(f_{e,q} + f_{h,q}),\\ &= \Delta E_{gCH} + \Delta E_{gSX},\end{aligned}$$

where ΔE_{gSX} screened exchange correlation and ΔE_{gCH} is the Coulomb hole contribution. For 3D, ΔE_{gCH}, Coulomb hole contribution is given by

$$\Delta E_{gCH} = -\frac{2E_0 a_0 \kappa}{\left[1 + C^{1/2}\left[\frac{E_0}{\hbar\omega_{pl}}\right](a_0\kappa)^2\right]^{1/2}}.$$

The screened exchange term is integrated numerically. However, there does not exist a recipe for the value of numerical constant C for an arbitrary material. This reduces the applicability of this approximation for in general materials.

5.2 Vashishta-Kalia Model

Vashishta and Kalia (VK model) simplified the exchange and correlation energy for p-n type materials and showed that the band gap renormalization is independent of the band characteristics [34]. However, further studies showed that in wide-gap semiconductors such as II-VI group elements, VK model deviates from experimental results [35].

Vashishta and Kalia simply fitted [34] the exchange and the correlation energy of the semiconductors to the expression

$$\varepsilon_{xc} = \frac{a + br_s}{c + dr_s + r_s^2},$$

where

$$\begin{aligned}a &= -4.8316,\\ b &= -5.0879,\\ c &= 0.0152,\\ d &= 3.0426.\end{aligned}$$

r_s is the dimensionless inter-particle distance, which is defined in terms of carrier density n, static dielectric constant ε and effective bohr radius $a_B^* = \hbar^2\varepsilon/\mu e^2$

$$\frac{4\pi}{3}(a_B^* r_s)^3 = \frac{1}{n}.$$

What we expect is that VK model would fit to the recent experimental data

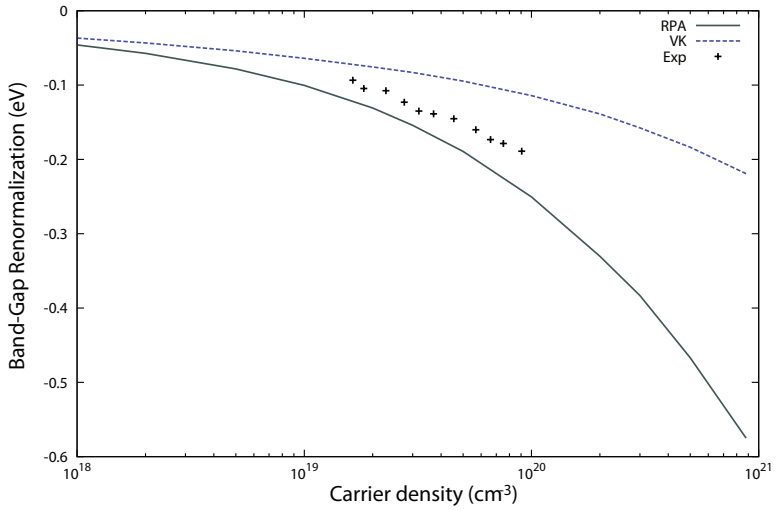

Figure 5.1: The dashed lines are the VK formulation for the band gap renormalization. Solid lines are the formulation of Sernelius approach. The symbol points are taken from the experimental data in Ref. [36].

for GaN since GaN is an III-V group compound as InN. It was experimentally shown that for GaN the band gap renormalization is temperature (T) independent [36]. This independency makes GaN a good sample to check the validity of the VK model up to plasma densities for an arbitrary temperature. For GaN we calculated the density dependent effective masses for both holes and electrons. As static dielectric constant, 9.5 is used. According to the VK model we get ΔE_{BGR} of GaN as a function of $e-h$ density, n between a range of $1{\times}10^{18}$ and $1{\times}10^{21}$ as shown in Fig. 5.1. When we compare our calculation with the data taken from Ref. [36], we observe that VK model deviates from the experimental data significantly. For further calculations such as the refractive index, VK model loses its validity at this range of the carrier density for our purposes.

5.3 Random Phase Approximation

For heavily doped n-type materials, the electron-electron and electron-ion contributions are well estimated by the random phase approximation (RPA). The contributions are defined by the following formulas

$$\Delta E_{c-c} = -\frac{2e^2 k_F}{\pi\epsilon_0} - \frac{e^2 k_{TF}}{2\epsilon_0}\left[1 - \frac{4}{\pi}\arctan\left(\frac{k_F}{k_{TF}}\right)\right],$$

$$\Delta E_{c-i} = -\frac{4\pi e^2 n}{\epsilon_0 a_B^* k_{TF}^3},$$

where n is the carrier density, ϵ_0 is the static dielectric constant,

$$k_F = \left(3\pi^2 n\right)^{1/3},$$

is the Fermi wave number,

$$k_{TF} = 2\sqrt{k_F/(\pi a_B^*)},$$

is the Thomas-Fermi wave number, a_B^* is the effective bohr radius, which uses m_e^* for the conduction band effective carrier mass. For n-p type of GaN, we modified the effective carrier mass into reduced effective e-h masses μ_x. It is first seen in Fig. 5.1 that the deviation of n-type GaN from n-p type GaN is not significant. The experimental data in Ref. [36] has good agreement with n-p type GaN and far away from the VK approximation.

For both n-doped and photoexcited InN we obtain the band gap renormalization as shown in Fig. 5.2. Due to lack of photoexcited InN experimental data, we only compare it with the n-doped InN. Experimental data taken from different references is not far away from RPA results. The correlation of both type InN's leads us to examine the behaviour of the n-p type InN. VK model again deviates from the RPA. The data taken from Ref. [39] is for Cubic InN. It is known that cubic InN has lower band gap compared to wurtzite InN. This can be the reason for the small deviation from our data. We can conclude that the difference between n-type material and p-n type material is not significant. Since the effective masses of the holes are too heavy compared to the conduction band edge electrons masses, they behave as fixed ions.

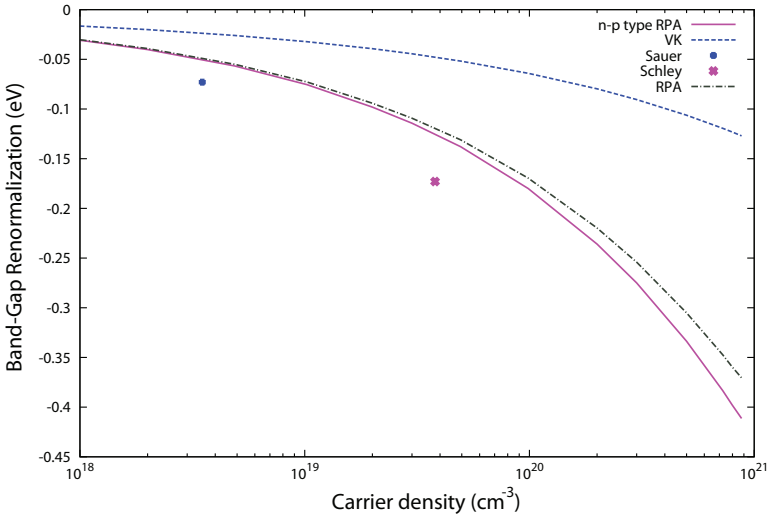

Figure 5.2: Band gap renormalization for different types of InN with different type of methods.

5.4 Band Tailing Effect

Even though we shall not consider in the remaining part of this thesis, for completeness , we want to mention the band tailing effect. This phenomenon occurs especially in heavily p-doped semiconductors. Acceptors and the donors are responsible for the free carriers in both valence and conduction bands. In this n-p type of semiconductors, we observe band tailing effect besides the discussed effects in the preceding sections. We define the band tailing as the perturbative change of the conduction (E_c) and valance bands (E_v). A new continuum states is formed above the E_v and the below the E_c and these states have important consequences for the absorption, radiation processes. And these states tend to decrease the band gap of the material as correlation and exchange energies have done since the density of states penetrate into the forbidden gap. The main idea under this phenomenon is the randomly distribution of the impurities. Gaussian distribution is the one of the approach. And this tail effect should be considered during the band gap renormalization calculations [37]. We can define this effect

with,

$$G = 2\sqrt{\pi}\frac{4\pi e^2}{\varepsilon R_s}(N_i R_s^3)^{1/2},$$

where

$$R_s = \frac{a_{Be}}{2}(n a_{Be}^3)^{-1/6},$$

is the Thomas-Fermi screening length, a_{Be} is the effective Bohr radius of electron, $N_i = [(1+K)/(1-K)]\, n$ is the total ionized impurity concentration, K is the compensation ratio and n is the carrier density. Since the holes have greater effective mass which results with the smaller R_s, the contribution comes from the holes can be disregarded. The tail states localized at the minima of the valence band so the shrinkage of the band gap is than stated as [38]

$$G^* = -E_v + \sqrt{2}G - kT/2.$$

As it is not relevant to our work, we do not include these formulations in the rest of our calculations.

Chapter 6

Refractive Index Change with Burstein-Moss Effect

Burstein-Moss effect and band gap renormalizations are the two phenomena that cause a shift in the quasi-Fermi level of the both conduction band and valence bands. While the Burstein Moss effect increases the Fermi level of the conduction band, band gap renormalization partially cancels this effect and tries to restore the original band gap of the semiconductor. Burstein-Moss effect is inversely proportional with the effective mass of the carriers as mentioned in the relevant chapter. So it is expected that Burstein-Moss prevails in such semiconductors that cause a strong blue shift in the absorption edge. Both of these effects do not only change the absorption edge of the semiconductor but they also change the optical properties of the medium through the causality principle. Once we obtain the imaginary part of the dielectric tensor, by using the Kramers-Kronig relation we can get the real part of the dielectric function.

6.1 Electronic Structures

InN and GaN belong III-IV group semiconductors. Based on Ref. [50] their band structures are obtained as shown in Fig. 6.1. These calculations are done by

using the *pseudopotential method*. To give a brief explanation for this method, we should first look at the structure of the atoms that constitute the semiconductor. The electrons of an atom can be energetically divided into two classes: the core electrons are strongly bonded to the atom, whereas the valence electrons are loosely bound. Valence electron wave functions are orthogonal to the those of the core electrons. This necessitates their wave functions to be highly oscillatory in the core region. So the wave functions of the valence electrons can be split into a pseudo-wave function (smooth) and an oscillatory part. Since the valence electrons exposes a repulsive force near the core electrons, one can approximate the true potential by psuedopotential (weaker effective potential). By fitting the experimental data to the pseudopotential factors which is known as the *empirical pseudopotential method*, one can mimic the true potential. As the most of the physical properties of the materials depend on the valence and conduction electrons, this makes a viable route to calculate optical properties of the semiconductor [51].

6.2 Brillouin Zone Integration

By using the Lehmann-Taut method, we computed the available density of states for InN shown in the Fig. 6.2. For this calculation we divide the irreducible Brillouin zone into a mesh of $40 \times 40 \times 40$ along the basal plane and the c-axis. For different carrier densities, we fill the available states of the both conduction band and valence band and we identify the quasi-fermi levels of these bands. Dramatic change in the fermi level of the bands can be seen in the inset graph 6.2. Essentially all of the shift comes from the electrons. This is because electrons have much lighter effective masses compare to the holes. Once we have calculate the fermi levels, next we renormalize the band gap. These calculations are based on the random phase approximation and we use reduced excitonic effective masses.

Taking both Moss-Burstein effect and band gap renormalization into account, the corresponding quantity for the absorption edge is the imaginary part of the

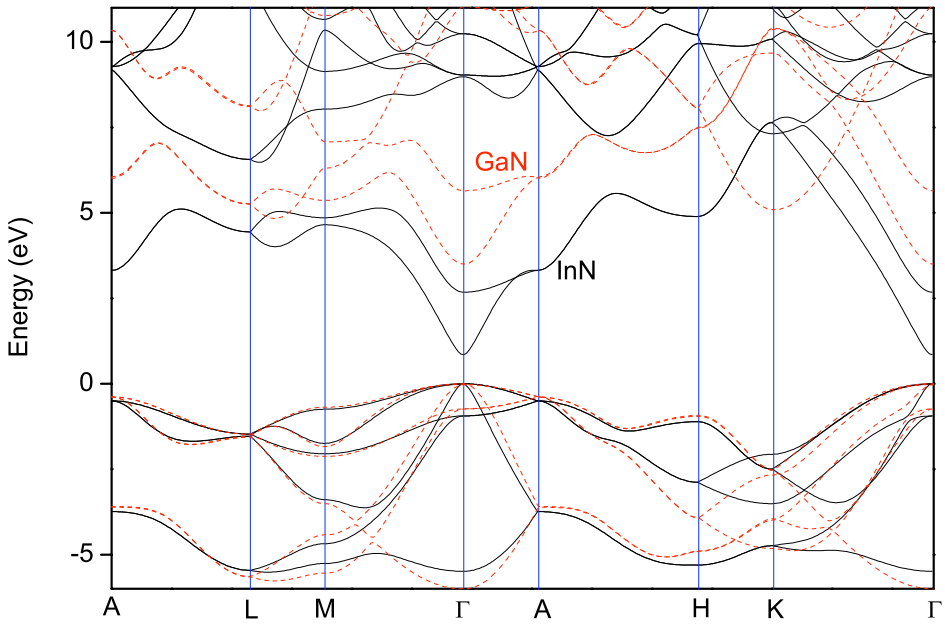

Figure 6.1: Band structure of InN (solid) and GaN (dashed) computed by using empirical pseudopotential method [50].

optical dielectric tensor which is given in Gaussian units as,

$$Im\left\{\epsilon^{ab}(\omega)\right\} = \frac{e^2}{\pi}\sum_{v,c}\int_{BZ} d\mathbf{k}\,\mathbf{r}^a_{vc}(\mathbf{k})\mathbf{r}^b_{vc}(\mathbf{k})\mathbf{r}^a_{vc}(\mathbf{k})\delta\left(E_c(\mathbf{k}) - E_v(\mathbf{k}) - \hbar\omega\right),$$

where a, b are the Cartesian indices. $r^a_{vc}(\mathbf{k}) = p^a_{vc}(\mathbf{k})/\left(im_0\omega_{vc}(\mathbf{k})\right)$, where $p^a_{vc}(\mathbf{k})$ is the momentum matrix element, m_0 is the free electron mass, $\omega_{vc}(\mathbf{k}) = \omega_v(\mathbf{k}) - \omega_c(\mathbf{k})$, where $\hbar\omega_n(\mathbf{k}) = E_n(\mathbf{k})$ is the energy of the band n, at the wave vector $\mathbf{k}$. The Dirac delta term in the integration reduces the volume integration to the surface integral formed by the $\mathbf{k}$-points that allow direct transitions from the valence band to the unfilled part of the conduction band with an energy difference corresponding to the chosen photon energy. The constant energy surface integral over the irreducible Brillouin zone is taken again by using Lehmann-Taut method.

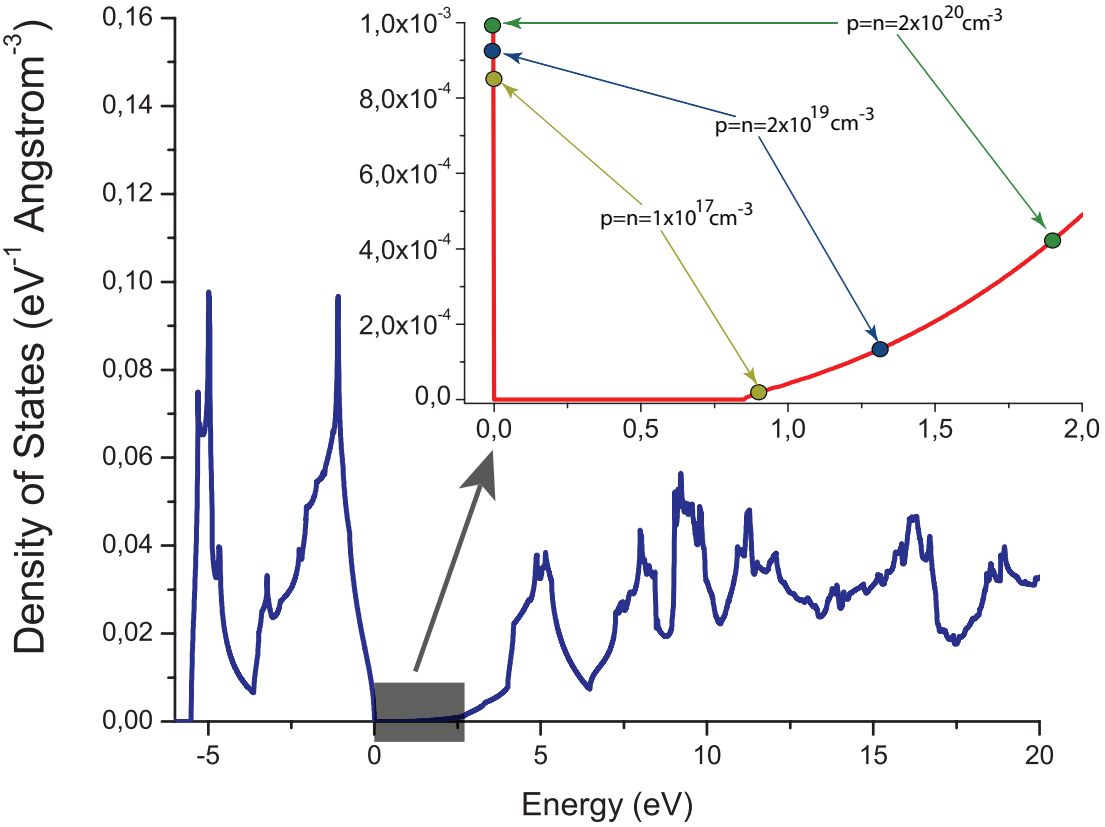

Figure 6.2: Density of states for InN. The inset gives us a view in a narrow energy range for DOS. Band filling effect is given for different carrier densities.

6.3 Results

The result is shown in the following Fig. 6.3. Here, the prominent behaviour of the absorption of the medium is the peaks around 0.9 eV. As the carrier density increases these peaks diverge. This is a result of Van Hove singularities as mentioned in section 3.4. Now let' s identify this transition on the band structure of InN. Figure 6.4 shows the available interband and intraband transitions. As shown in Fig. 6.4b, absorption of a photon with an energy 0.9 eV results in the excitation of an electron from band Γ_5^v to Γ_6^v. These peaks dominate the absorption of the medium in this energy range hence the associated refractive index change.

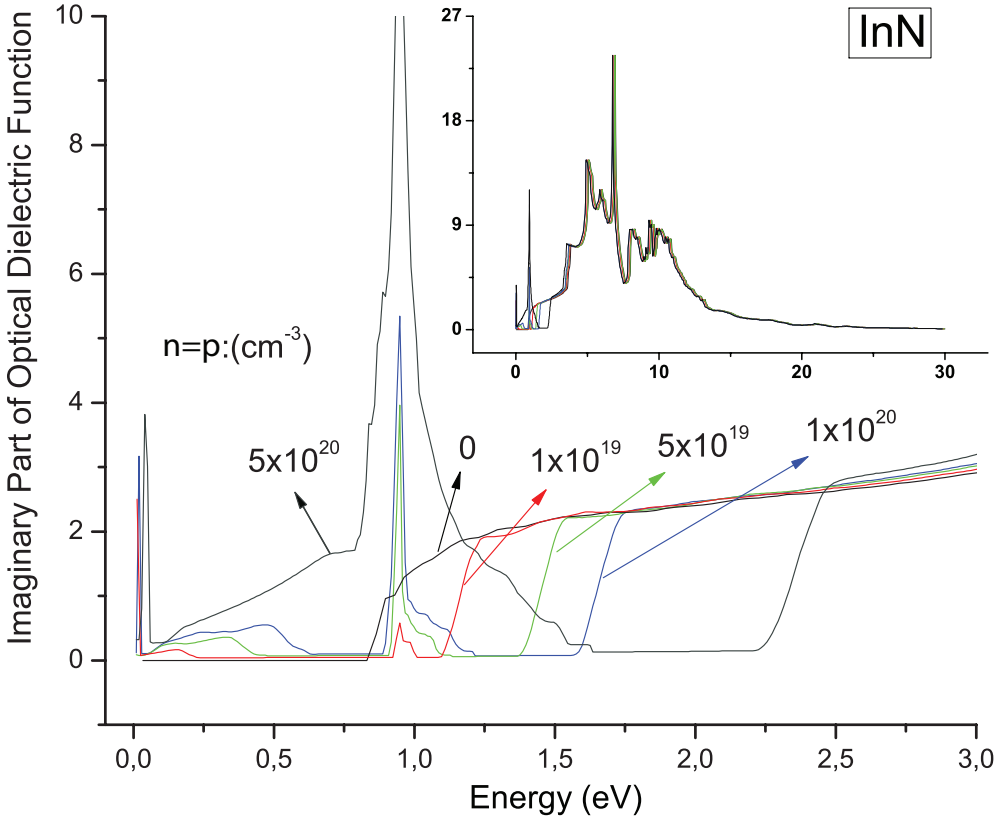

Figure 6.3: Imaginary part of the dielectric function of InN. The inset shows the behaviour of the function in a wider energy range.

Having determined the imaginary part of the dielectric function, our next aim is to compute the real part of the dielectric function. The relationship between the real part of the dielectric function with the imaginary part is established by the Kramers-Kronig relation. For our objectives, the corresponding expression for the real part of the dielectric function is given by the following formula,

$$Re\left\{\epsilon(\omega)\right\} = 1 + \frac{2}{\pi} P \int_0^\infty \frac{\omega' Im\left\{\epsilon(\omega')\right\}}{\omega'^2 - \omega^2} d\omega'.$$

Upper integration limit indicates the knowledge of the imaginary part of the dielectric function up to very high limits. So the integral is taken up to 60 bands corresponding energy value is above 30 eV. Beyond this energy we perform the integral analytically with a $1/\omega^2$ fall off. The result of the integral is shown in Fig. 6.5.

Now we are able to compute the refractive index change as result of Burstein

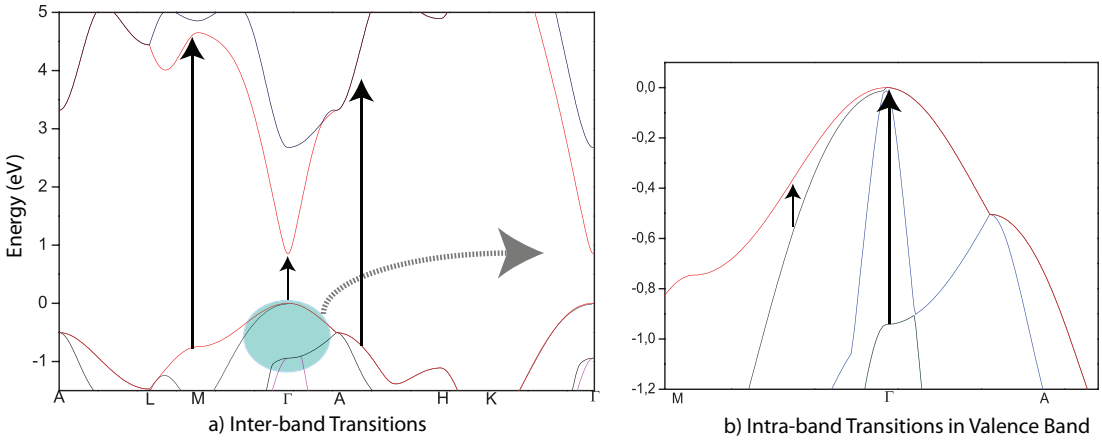

Figure 6.4: A basic illustration for the transitions of electrons by absorbing photons. a shows interband transitions and b shows intraband transitions.

Moss effect and band gap renormalization. By using the relationship between the refractive index and dielectric function we can reach the modified refractive index. The relation is given by the following formula [53],

$$n = \sqrt{\frac{\sqrt{Re\{\epsilon\}^2 + Im\{\epsilon\}^2} + Re\{\epsilon\}}{2}}.$$

We should note that this also includes the contribution from the free carriers (plasma) using the Drude expression which is in the form

$$\Delta n \approx \frac{-N_x e^2 \lambda^2}{8\pi^2 \epsilon_0 n c^2 m_x^*},$$

with energy dependent excitonic effective masses. The refractive index change of n-type and n-p type InN for a photon energy 0.8 eV (or a wavelength 1.55 μm) is given in the Fig. 6.6.

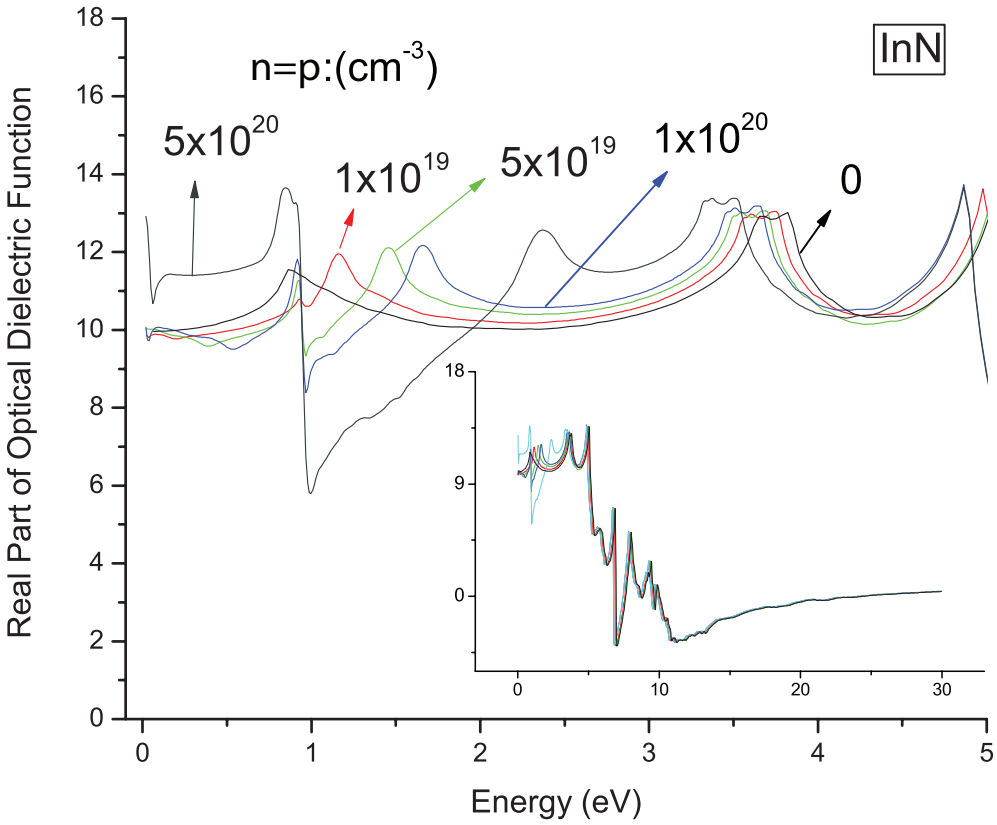

Figure 6.5: Real part of the dielectric function of InN. The inset shows the behaviour of the function in a wider energy range.

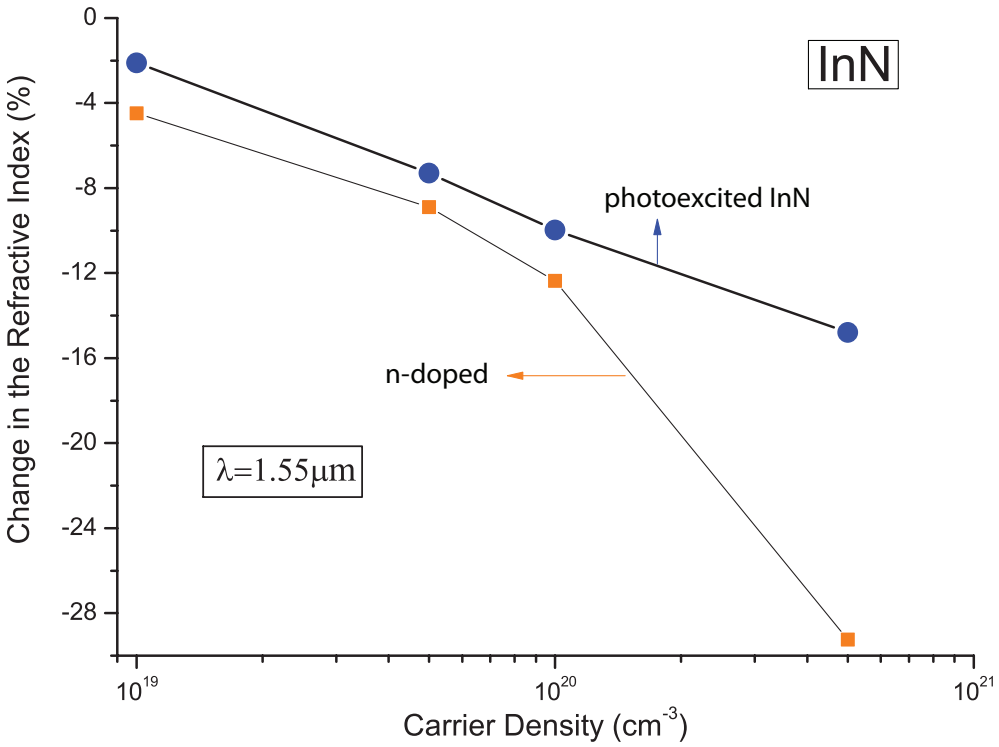

Figure 6.6: Carrier density dependent change in the refractive index of n-doped and photoexcited ($n = p$) InN for a photon energy 0.8 eV .

Chapter 7

Conclusion

Based on the full band structure of the InN, we explored the filling of the conduction band by photo-injection. Increasing photon absorption, increases the transition from valence band to conduction band and the excited electrons leaves holes behind in the valence band. So we generate both n and p-type carriers in InN. This is also the basic underlying principle of semiconductor lasers. Under photonic pumping we consider carrier concentrations up to about 5×10^{20} cm^{-3} so that only the lowest conduction band is filled. Pauli principle excludes the electrons (as well as holes) to be at the same energy state at the same time, so electron needs more energy to reach to available states.

As the carrier concentration in both valence and conduction bands increases, due to many body effects the band gap of the semiconductor shrinks and this effect is calculated by using RPA. Both these effects affect the absorption edge shift. However, we neglect excitonic effects in the absorption edge. By adding the plasma contribution, we reach the overall change in the refractive index for the wavelength of 1.55 μm since it has technological importance. For both n-doped and photoexcited InN, band gap renormalizition partially cancels Moss-Burstein effect. On the other hand, negative plasma contribution become important for the carrier densities above 1×10^{19} cm^{-3}. For photoexcited InN, intra-band transitions caused by the Van Hove singularities somewhat mast this the refractive index change. As the carrier densities further increases, the opened $\Gamma_5^v \rightarrow \Gamma_6^v$

transitions negate the Burstein Moss effect and band gap renormalization contribution and at a carrier density 1×10^{20} cm^{-3} the negative effect totally turns into positive as a sum. However after this concentration the plasma contribution dominates the refractive index change and the obvious difference between n-doped and photoexcited InN can be seen figure 6.6.

We predict about 9 % change in the refractive index for InN for a carrier density about 10^{20} cm^{-3} and 6 % change for a carrier density of 5 $\times10^{19}$ cm^{-3}. Also the linear behaviour of the refractive index change dependent on the carrier concentration makes the system more predictable for different densities. This wide tunability of the refractive index under different densities should be considered for the InN based semiconductor lasers and also for the application to the optical modulators, warrants further study.

Bibliography

[1] M. Tanenbaum, H. B. Briggs, Phys. Rev. **91,** 1561 (1953).

[2] E. Burstein, Phys. Rev. **93,** 632 (1954).

[3] T. S. Moss, Proc. Phys. Soc. B **67,** 775 (1954).

[4] P. D. Dapkus, N. Holonyak, J. A. Rossi, F. V. Williams, D. A. High, J. Appl. Phys. **40,** 3300 (1969).

[5] H. C. Casey, D. D. Sell, K. W. Wecht, J. Appl. Phys. **46,** 250 (1975).

[6] M. Carroll, P. Blood, T. Ashley, C. T. Elliott, IEE Proc.-Optoelectron. **147,** 157 (2000).

[7] D. G. Deppe, N. D. Gerrard, C. J. Pinzone, R. D. Dupuis, E. F. Schubert, Appl. Phys. Lett. **56,** 315 (1989).

[8] K. L. Vodopyanov, A. V. Lukashev, C. C. Philips, I. T. Ferguson, Appl. Phys. Lett. **59,** 1659 (1991).

[9] J. H. Abeles, W. K. Chan, E. Colas, A. Kastalsky, Appl. Phys. Lett. **54,** 2177 (1989).

[10] F. X. Zha, J. Shao, J. Jiang, W. Y. Yang, Appl. Phys. Lett. **90,** 201112 (2007).

[11] J. W. Trainor, K. Rose, J. Electron. Mater. **3,** 821 (1974).

[12] T. L. Tansley, C. P. Foley, J. Appl. Phys. **59,** 3241 (1986).

[13] J. Wu, W. Walukiewicz, K. M. Yu, J. W. Ager, E. E. Haller, H. Lu, W. J. Schaff, Y. Saito, Y. Nanishi, Appl. Phys. Lett. **80,** 3967 (2002).

[14] A. G. Bhuiyan, A. Hashimoto, A. Yamamoto, J. Appl. Phys. **94,** 2779 (2003).

[15] R. D. Guenther, *Modern Optics*, Wiley New York (1990).

[16] B. E. A. Saleh, and M. C. Teich, *Fundamentals of Photonics,* New York: John Wiley & Sons (1991).

[17] M. Bass, E.W.V Stryland, D.R. Williams, W.L. Wolfe, *Handbook of Optics Volume II Devices, Measurements, and Properties* McGraw-Hill Professional (1995).

[18] J. W. Goodman, *Introduction to Fourier Optics*, Robert & Co (2005).

[19] C. F. Klingshirn, *Semiconductor Optics*, Springer (2005).

[20] P. Tayebati, Appl. Phys. Lett. **63,** 2878 (1993).

[21] S. H. Kwok, H. T. Grahn, K. Ploog, R. Merlin, Phys. Rev. Lett. **69,** 973 (1992).

[22] A. A. Toropov, E. L. Ivchenko, O. Krebs, S. Cortez, P. Voisin, J. L. Gentner, Phys. Rev. B **63,** 035202 (2000).

[23] B. E. Sernelius, K. F. Berggren, Z. C. Jin, I. Hamberg, C. G. Granqvist, Phys. Rev. B **37,** 10244 (1988).

[24] S. Noda, M. Fujita, T. Asano, Nature, **1,** 449 (2007).

[25] J. M. Gerard, B. Gayral, Journal of Lightwave Technology, **17,** 11 (1999).

[26] J. M. Gérard, B. Sermage, B. Gayral, B. Legrand, E. Costard, V. T. Mieg, Phys. Rev. Lett. **81,** 1110 (1998).

[27] D. A. B Miller, D. S. Chemla, T. C. Damen, A. C. Gossard, W. Wiegmann, T. H. Wood, C. A. Burrus, Phys. Rev. Lett. **53,** 2170 (1984).

[28] J. Hader, N. Linder, G. H. Döhler, Phys. Rev. B **55,** 6960 (1997).

[29] D. A. B. Miller, D. S. Chemla,S. S. Rink, Phys. Rev. B **33,** 6976 (1986).

[30] C. Kittel, *Introduction to Solid State Physics,* John Wiley-Sons, Inc. Press.

[31] A. Szabo, N. S. Ostlund, *Modern Quantum Chemistry*: Introduction to Advanced Electronic Structure Theory, Dover Publications, New York.

[32] H. Haug, S.W. Koch, Phys. Rev. A **39,** 4 (1989).

[33] J. Linhard, K. Dan. Vidensk. Selsk. Mat.-Fys. Medd. **28,** 8 (1954).

[34] P. Vashista, R. K. Kalia, Phys. Rev. B **39,** 6492 (1982).

[35] H. E. Swoboda, M. Sence, F. A. Majumder, M. Rinker, J. Y. Bigot, J. B. Drun, C. Klingshirn, Phys. Rev. B **39,** 11019 (2002).

[36] T. Nagai, T. J. Inagaki, Y. Kanemitsu, Appl. Phys. Lett. **84,** 1284 (2004).

[37] B. Arnaudov, and T. Paskova, P.P. Paskov, B. Magnusson, E. Valcheva, B. Monemar, H. Lu, W.J. Schaff, H. Amano, and I. Akasaki, Phys. Rev B **69,** 115216 (2004).

[38] B. Arnaudov, and T. Paskova, E.M. Goldys, S. Evtimova, B. Monemar, Phys. Rev B **64,** 045213 (2001).

[39] P. Schley, R. Goldhahn, C. Napierala, G. Gobsch, J. Schormann, D. J. As, K. Lischka, M. Feneberg, K. Thonke, Semicond. Sci. Technol. **23,** 055001 (2004).

[40] G. Gilat, L. J. Raubenheimer, Phys. Rev. **144**, 390 (1966).

[41] D. Lipton, R. L. Jacobs, J. Phys. C:Metal Phys Suppl, **3** (1970).

[42] G. Lehhman, M. Taut, Phys. Stat. Sol.(b) **54**, 469 (1972).

[43] J. S. Blakemore, *Semiconductor Statistics*, Dover Publications, Inc. (1987).

[44] F. Bassani, G. P. Parravicini, R. A. Ballinger, *Electronic States and Optical Transitions in Solids*, Pergamon Press, (1975).

[45] N. M. Ashcroft, N. D. Mermin, *Solid State Physics*, Saunders College Publishing, (1976).

[46] T.H. Maiman, Nature, **187**, 493 (1960).

[47] E. Kapon, *Semiconductor Lasers I, Fundamentals*, Academic Press (1998).

[48] S. L. Chuang, *Physics of Optoelectronic Devices*, Wiley-Interscience publication, Cambridge (1995).

[49] T. Numai, *Fundamentals of Semiconductor Lasers*, Springer (2004).

[50] C. Bulutay, B. K. Ridley, N. A. Zakhleniuk, Phys. Rev. B **62,** 15754 (2000).

[51] E. F. Schubert, *Doping in III-IV Semiconductors*, Cambridge University Press (2003).

[52] M. Dressel, G. Gruner, *Electrodynamics of Solids:Optical Properties of Electrons in Matter*, Cambridge University Press (2002).

[53] F. Wooten, *Optical Properties of Solids*, Academic Press (1972).